university of groningen

faculty of science and engineering

Oxidation States in Gold Complexes: a Computational and Spectroscopic Study

Bachelor's thesis in Physics

June 2021

Student: A. Volker

Primary supervisor: Prof. Dr. M. Tromp

Secondary supervisor: Prof. Dr. P. Rudolf

Abstract

A study of various gold complexes with formal oxidation states of +1 and +3 using XES and computational methods is presented. Three different DFT methods, B97-3c, B97-D3/def2-TZVP and B97-D3 ZORA/def2-TZVP, were found to give comparable geometries. Orbital localization using the Pipek-Mezey scheme was performed for all three methods. Significant difference were found when using the all-electron ZORA method with respect to the methods that use ECPs. For complexes with a higher oxidation state the localized bond orbitals showed a higher charge on the gold atom. Laboratory based XES measurements on the Lβ_5 and Lβ_3 transition were done for 5 of the complexes using the EasyXES100 spectrometer. No shift in position of the peaks was found at the level of resolution obtained in this experiment. The cancelling effect of covalency could explain why no shift was observed. Potential improvements on these experiments are discussed.

Acknowledgments I would like to thank Prof. Dr. M. Tromp for her support and for the opportunity to do the project within her research group, Isaac Leach for the daily supervision and help during the projects and the Klein group for kindly providing samples for the XES measurements.

Contents

1 Introduction

A major goal in chemistry is the understanding of reaction mechanisms. Especially of interest is the understanding of the many transition metal (TM) catalysts, which can undergo one- or two-electron redox reactions. Understanding the electronic structure of such transition metal complexes provides an essential step towards the design of new and possibly better catalysts. One fundamental way in which chemists communicate about the electronic structure and chemical reactivity is the concept of the oxidation state [1]. The term oxidation is not without controversy. For years the way to determine the *formal* oxidation state was specified, no exact definition was given. The term oxidation state is derived from the number of oxygen atoms that an element can bind to, as described by F. Wöhler [2] in the 19th century. It is now no longer related to oxygen and is a purely formal concept. There has been considerable debate on the inconsistencies, misconceptions and usefulness of concept [3–5]. In 2009, a task group was set up by IUPAC to tackle the conundrum. In 2014 a report was published [6], which included a new generic definition and hundreds of examples. The generic definition of the *formal* oxidation state is now "the atom's charge after ionic approximation of its heteronuclear bonds". This formalism has received criticism for not discussing the connection to quantum chemical calculations [7].

When looking at TM complexes, the ligands do not necessarily possess a closed shell configuration and there might be a significant covalent character to the bond [8]. This so-called *noninnocence* of ligands makes the assignment of a clear oxidation state increasingly more challenging [7]. Besides the *formal* oxidation state, another term that is often coined when discussing transition metal complexes is the *physical* or *spectroscopic* oxidation state. This refers to the better measurable quantity of the number n of a d^n configuration [9]. X-ray spectroscopy has become an important tool to investigate the oxidation states of TM complexes, due to its element selectivity and involvement of core electrons [1]. In X-ray spectroscopy, a high-energy photon interacts with a sample and is used to excite a core electron. In X-ray absorption spectroscopy (XAS) a core electron is promoted to an empty orbital and thus "probes the empty molecular orbitals". X-ray emission spectroscopy (XES) is based on the emission of a photon when an electron decays to a previously created core hole, thus "probing the occupied molecular orbitals" [10]. The two methods give complementary information.

3d-transition metal complexes, as well as some 4d metals, have been studied extensively using both XAS and XES as well as computational studies [11]. Valence to core XES is particularly interesting for TM complexes, as the character of those valence orbitals changes the most upon changing the ligand, making it a highly ligand sensitive method [12]. Lee et al. [13] showed in a systematic experimental and computational study of ferrous and ferric complexes a profound sensitivity to the chemical environment of these transitions, which could also be modelled well with straightforward DFT studies. This year Castillo et al. demonstrated the ability of resonant XES to even better differentiate between different oxidation states in ferrous and ferric complexes [1]. Ravel et al. [14] published a study on the 4d metal Nb, where they clearly showed the ligand dependency of the Kβ" peak (ligand 2s electron to Nb 1s core hole) experimentally. They also suggested a chemistry dependence of the Kβ_4 (Nb 4d to Nb 1s), similar to what is seen for Mo by Doonan et al. [15]. For 5d metals, there is less information available, but a study by Prydachenko [16] showed that for the 5d to 2p (Lβ_5) transition in Pt and Au theoretical calculated local partial densities of electronic states (LPDOS) on the noble atom and on the neighboring ligands and experimental spectra showed good agreement. For a

more detailed review of valence-to-core XES and its applications the reader is referred to [17].

Gold is a 5d metal, making gold complexes very interesting for these studies as 5d metals have generally been studied less using XES. The gold complexes studied in this bachelor thesis show a variety of types of ligands, formal oxidation states and sizes. Based on availability and time constraints the complexes numbered 3, 7, 8, 9 and 11 are studied using both using XES and DFT, while the other complexes are only studied computationally. In the computational study, the goal was not to simulate the spectra but to investigate the localized molecular orbitals to gain a better understanding of the metal-ligand bonds and electronic structure of those complexes. This way it can be investigated what information the simpler ground state calculations can already provide on the electronic structure and how this might relate to the XES spectra of the gold complexes. For calculations of the XES spectra, the inclusion of relativistic effects through all-electron methods has shown to give better agreement for 3d metals [18]. With gold being heavier, the inclusion of scalar relativistic effects seems even more important. The influence on the localized bond orbitals of inclusion of scalar relativistic effects is investigated.

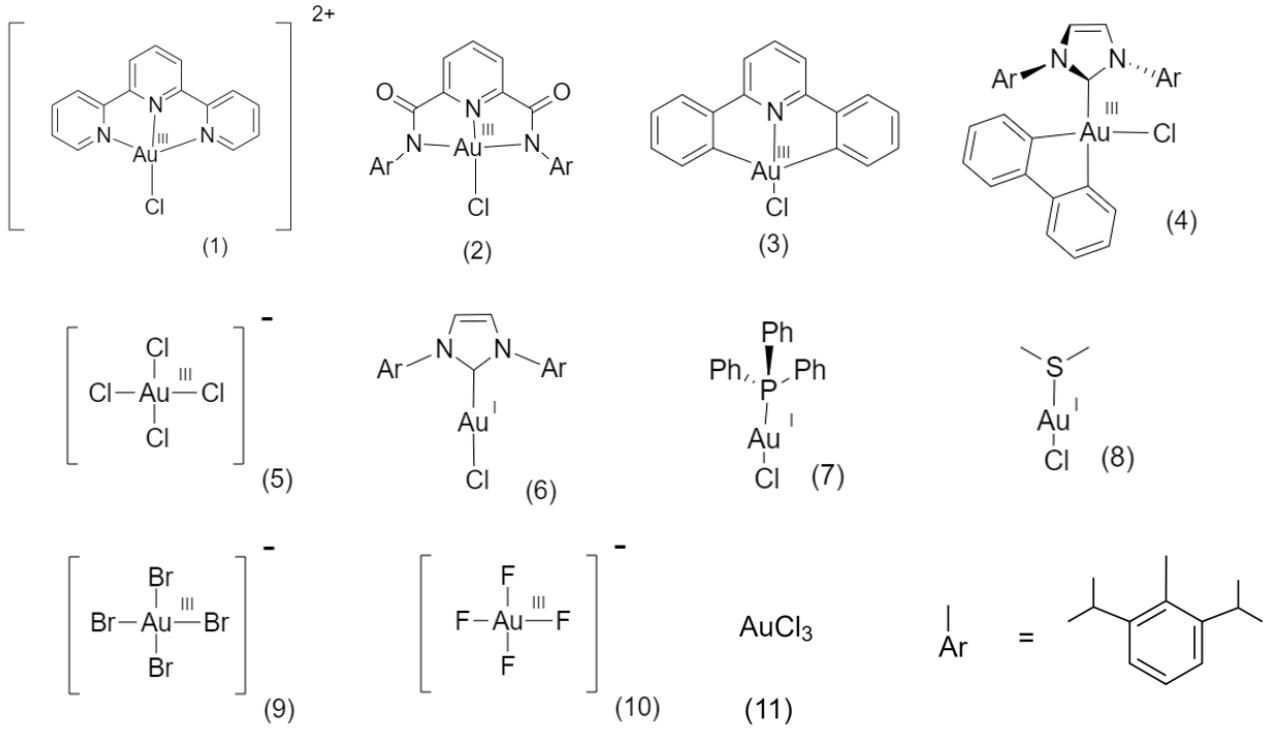

Figure 1.1: Overview of gold complexes studied

2 Theory

2.1 DFT

Computational schemes based on the Density Functional Theory (DFT) are among the most important and widely used methods in computational modeling of atoms, molecules and solids [19]. For an N-electron system, such as a large molecule or complex, the wavefunction is complicated. The wavefunctions depends on 3N spatical coordinates, as well as constraints to ensure the antisymmetrical nature of the wavefunction. For most calculations however, not the wavefunction itself, but the probability that a set of N electrons can be found at certains positions, regardless of order, is of physical interest. This is related to the electron density $\rho(\mathbf{r})$:

$$\rho(\mathbf{r}) = N \int \Psi^*(\mathbf{r_1}, \mathbf{r_2}, ..., \mathbf{r_N}) \Psi(\mathbf{r_1}, \mathbf{r_2}, ..., \mathbf{r_N}) d\mathbf{r_1} d\mathbf{r_2}, ..., d\mathbf{r_N} \tag{2.1}$$

DFT is based on this electron density which is a three-dimensional function, making it often computationally cheaper than wavefunctions based methods. This holds especially for large systems, such as some of the gold complexes investigated in this thesis. As any quantum chemical calculation, the final result will still give you to molecular orbitals of your system. In this thesis calculations on a variety of gold complexes are done using DFT methods. As the complexes involve heavier transition metals, the inclusion of (scalar) relativistic effects can be of importance. In the section firstly an overview of non-relativistic DFT is given (based on [19–22]) and secondly different methods of including relativistic effects are discussed.

2.1.1 Hohenberg–Kohn theorems

The basis of DFT are the theorems Hohenberg and Kohn developed in the mid-60's [23]. The first theory states that *The ground-state energy from Schrödinger's equation is a unique functional of the electron density.* This statement tells us that all the information needed to determine the properties of the ground state, such as energy and wavefunction, are contained in the electron density. the second theorem states that *the ground-state electron density can be found variationally*, analogous to the Rayleigh-Ritz principle. The electron density that minimizes the energy is the electron density corresponding to the ground state. Up until here, there is no guarantee that finding this electron density is any easier than solving the Schrödinger equation.

The energy functional, E[ρ], can be given as the sum of different contributions, as one would for a Hamiltonian:

$$E[\rho] = T[\rho] + E_{eN}[\rho] + J[\rho] + E_{XC,i}[\rho] \tag{2.2}$$

with $E_{eN}[\rho]$ being the electron-nuclei interaction

$$E_{eN}[\rho] = \sum_A \int \frac{Z_A \rho(\mathbf{r})}{|\mathbf{r_A} - \mathbf{r}|} d\mathbf{r} \tag{2.3}$$

and $J[\rho]$ representing the Coulomb repulsion between electrons

$$J[\rho] = \frac{1}{2} \iint \frac{\rho(\mathbf{r})\rho(\mathbf{r'})}{|\mathbf{r} - \mathbf{r'}|} d\mathbf{r} d\mathbf{r'} \tag{2.4}$$

The kinetic energy $T[\rho]$ and the exchange-correlation energy for the interacting system $E_{XC,i}[\rho]$ are not known and any attempts to give the explicit functional for the kinetic energy have as of yet been unsuccessful.

2.1.2 Kohn–Sham equations

This problem was solved a year later when Kohn and Sham [24] published the Kohn-Sham equations which use a system of non-interacting electrons. Then an external potential field is formed, such that the electron density of this hypothetical system is equal to the true, and unknown, electron density of the ground state. Since there are no interactions between the electrons in this system, the Hamiltonian can be written as:

$$H^{ref} = T^{ref} + V^{ref} = \sum_i \left[-\frac{1}{2}\nabla_i^2 + v_{eff}(\mathbf{r_i}) \right] \tag{2.5}$$

From this Hamiltonian one can construct a set of one-electron Schrödinger equations, the Kohn-Sham equations. The solutions of which gives the lowest-energy eigenfunctions, the Kohn-Sham orbitals ϕ_i^{KS}. Using these orbitals the total electron density can be expressed:

$$\rho(\mathbf{r}) = \sum_i \phi_i^{KS}(\mathbf{r})^* \phi_i^{KS}(\mathbf{r}) \tag{2.6}$$

In the non-interacting case the kinetic contribution to the energy functional is known. This allows us to express the energy functional of the interacting system in terms of the reference system.

$$E[\rho] = T^{ref}[\rho] + E_{eN}[\rho] + J[\rho] + E_{XC}[\rho] \tag{2.7}$$

Here the kinetic energy of the interacting system is not equal to the one of the non-interacting one, but this difference $\Delta T = T[\rho] - T^{ref}[\rho]$ is absorbed in the $E_{XC}[\rho]$ term. Now the interacting system can be written if the form of eq. 2.5, with the effective potential being:

$$v_{eff}(\mathbf{r}) = v_{eN}(\mathbf{r}) + \frac{\delta J[\rho]}{\delta \rho(\mathbf{r})} + \frac{\delta E_{XC}[\rho]}{\delta \rho(\mathbf{r})} = v_{eN}(\mathbf{r}) + \int \frac{\rho(\mathbf{r}')}{|\mathbf{r} - \mathbf{r}'|} d\mathbf{r}' + v_{XC}(\mathbf{r}) \tag{2.8}$$

$v_{XC}(\mathbf{r})$ is the only unknown left in the equation. By starting with a trial function for the electron density and an appropriate $v_{XC}(\mathbf{r})$ a self-consistent solution to the KS equations can be found iteratively thanks to the Hohenberg-Kohn theorems.

2.1.3 Functionals

Although there is now a way to use solve the KS-equations, an exchange-correlation functional must be specified. Up to today, no explicit functional has been found and even if found, it would most likely be so complicated that all computational advantages of DFT are lost. So an approximate functional is used. Over the years hundreds of different functionals have been developed. In that sense, DFT should be seen as a collection of different methods. DFT calculations do not give exact solutions and results may differ between functionals [22]. There are many ways to divide functionals into groups, but an important distinction is between the non-empirical and semi-empirical functionals. Non-empirical functionals are based on know constraints of the exact functional and the more constraints included, the more accurate the functional [21]. Semi-empirical functionals have parameters fitted to to experimental or *ab initio* results. This gives them great accuracy for specific systems. Currently, the most widely used functionals are hybrid functionals that are a linear combination of the Hartree-Fock exact exchange functional and other exchange and correlation functionals, often ab initio or empirical.

The choice of a functional is a complex and often intimidating one. Benchmark studies bring some order in this "DFT zoo" and can help to make informed decisions on which functional to

use. Currently DFT calculations are often benchmarked against wavefunction-based *ab initio* results, such as CCSD(T) [25], instead of experimental data. This may seem puzzling, but experimental results also include vibrational, temperature and solvent effects. It is not the role of the functional to compensate for those per se [26]. While it is easy to just use one of the more well know functionals, such as B3LYP [27, 28], there are more things to consider. This does not by any means say that B3LYP might not be the right functional for a calculation, as it is well known and successful for a reason [22]. In the case of transition metals, as the complexes investigated in this thesis, local (non-hybrid) functionals are known to be rather robust [29]. Another thing to take into account is the inclusion of London dispersion forces, which is not correctly captured in most density functional approximations (DFA). One cost-effective way of including them is by additive corrections [26]. One of the more successful ways to do this is the DFT-D3 method by Grimme and coworkers [30]. Although a comprehensive discussion of different DFT methods that may be promising for transition metal complexes is outside the scope of this work, the reader is referred to [29, 31] for more details. One very promising method is the B97-3c [32] method developed by Grimme and coworkers. It is part of the "3c" family, which are cost-efficient composite methods specially developed for larger systems. For each 3c-method the least empirical exchange-correlation form is chosen that still gives competitive results. For the minimal basis set method HF-3c, short-range electron correlation is completely ignored, while PBEh-3c and HSE-3c can employ a slightly larger basis set and can use the semi-local description. B97-3c uses a triple-zeta basis set, which is large enough to include a more sophisticated exchange-correlation treatment. The B97-3c is the least empirical method of the 3c-methods and uses no Hartree-Fock exchange [33], making it a suitable choice for this project.

2.2 Relativistic Effects

The two theories that form the basis of modern physics are quantum mechanics and the theory of relativity. Modern-day (computational) chemistry would not exist without quantum mechanics. On the other hand, most main group chemistry can be treated very well without the inclusion of relativistic effects. This is however not the case for heavier elements; it is widely acknowledged that relativistic effects need to be included when describing electronic and molecular structures when 'heavier' atoms are involved [34, 35]. Relativistic effects can be defined as all effects, arising from the finite speed of light, instead of the infinite speed of light in the non-relativistic case [35]. A distinction can be made between the scalar-relativistic effects that arise from relativistic mass increase and the spin-orbit coupling. The former can be included in a non-relativistic framework, while spin-orbit coupling can not [36]. There are different ways to include relativistic effects in quantum chemical calculations, ranging from a fully four-component treatment to effective core potentials. The different methods come at different computational costs, often making an all-electron four-component treatment not preferable [34]. In this section, the basics of relativistic quantum chemical calculations are given as well as a description of different commonly used scalar relativistic methods.

2.2.1 Relativistic Hamiltonians

Relativistic effects are introduced through a relativistic Hamiltonian. Quantum electrodynamics (QED) provides the most general framework to discuss the interactions between electrons, but it is by no means a simple task to derive an appropriate Hamiltonian from QED. Since for example electron-positron pair creation plays no role in chemistry and other practical considerations, the Dirac-Coulomb-Breit Hamiltonian together with the Bohr-Oppenheimer approxi-

mation can be taken as the foundation of relativistic quantum chemistry [37, 38]:

$$H = \sum_i h_D(i) + \frac{1}{2}\sum_{i\neq j} g(i,j) + V_{NN}; \quad V_{NN} = \frac{1}{2}\sum_{A\neq B}\frac{Z_A Z_B}{R_{AB}} \tag{2.9}$$

The Hamiltonian consist of three parts, firstly the one- and two-electron interactions, described by respectively the one-electron Dirac Hamiltonian $h_D(i)$ and $g(i,j)$. The V_{NN} term gives the repulsion of classic nuclei.

$$h_D = \beta mc^2 + c(\boldsymbol{\alpha}\cdot\mathbf{p}) + V_{eN} \tag{2.10}$$

α and β are Dirac matrices, composed of the Pauli spin matrices and the identity matrix:

$$\alpha = \begin{pmatrix} 0 & \sigma \\ \sigma & 0 \end{pmatrix} \quad \beta = \begin{pmatrix} \mathbb{1} & 0 \\ 0 & -\mathbb{1} \end{pmatrix} \tag{2.11}$$

The two-electron interactions $g(i,j)$ are divided into the coulomb interaction and the Breit interaction:

$$g(i,j) = g^{Coulomb}(i,j) + g^{Breit}(i,j); \quad g^{Coulomb}(i,j) = \frac{1}{r_{ij}} \tag{2.12}$$

The Coulomb interaction includes the spin-ame orbit interactions in the relativistic case. The Breit interaction is usually further divided into the Gaunt interaction (spin-other orbit and spin-spin) and a gauge term (spin free interactions).

$$g^{Breit}(i,j) = g^{Gaunt}(i,j) + g^{gauge}(i,j) = -\frac{c\alpha_i\cdot c\alpha_j}{c^2 r_{ij}} - \frac{(c\alpha_i\cdot\nabla_i)(c\alpha_j\cdot\nabla_j)\, r_{ij}}{2c^2} \tag{2.13}$$

The gauge term is often neglected in calculations as it is smaller and more difficult to implement in calculations [37, 38].
Now it is important to mention that the Dirac equation describes both electrons and positrons and that spin emerges naturally due to the inclusion of the Pauli spin matrices [39]. Relativistic quantum mechanics is based on four-component spinors instead of one-component wavefunctions; each of these solutions can be written as a combination of two-component spinors:

$$\psi = \begin{pmatrix} \psi_L \\ \psi_S \end{pmatrix} \tag{2.14}$$

These components are called the large (L) and small (S) component, these names originating from the fact that for the solutions involving electrons, the large component is more important [39]. These two components are related by the so-called *atomic balance* [40]. From a computational perspective dealing with the Dirac Hamiltonian not only requires larger computational resources than the Schrödinger Hamiltonian but would also require to fundamentally rewrite the quantum chemistry codes in common software packages. Relativistic effects are often included as corrections in nonrelativistic software packages.

2.2.2 Zeroth Order Regular Approximation (ZORA)

Quite a few of methods to implement relativistic effects are based on eliminating the small component ψ_S. The following derivation is based on the explaination given in [39]. It can be shown, using the *atomic balance*

$$\psi_S(r) = K(\epsilon, r)\frac{\boldsymbol{\sigma}\cot\boldsymbol{p}}{2c}\psi_L(r); \quad K(\epsilon, r) = \left(1 + \frac{\epsilon - V}{2c^2}\right)^{-1} \tag{2.15}$$

that we can eliminate the small component by substitution:

$$\left(\frac{1}{2}(\boldsymbol{\sigma}\cdot\boldsymbol{p})K(\epsilon,r)(\boldsymbol{\sigma}\cdot\boldsymbol{p})+V\right)\psi_L(r)=\epsilon\psi_L(r) \tag{2.16}$$

To solve this equation one needs to find a way to express K(ϵ, r), for example by rewriting it as a geometric series:

$$K(\epsilon,r)=\left(1+\frac{\epsilon-V}{2c^2}\right)^{-1}=\sum_{k=0}^{\inf}\left(\frac{\epsilon-V}{2c^2}\right)^k \tag{2.17}$$

This works well for valence electrons, where the energy difference ϵ - V is much smaller than $2c^2$, but breaks down in the case of core electrons. The regular approximation, as introduced by Chang et al. [41] and further popularized by Van Lenthe et al. [42] within DFT, is a way to arrive at a series approximation that is valid over the whole region of space. The operator K is now written as:

$$K(\epsilon,r)=\left(1-\frac{V}{2c^2}\right)^{-1}\left(1+\frac{\epsilon}{2c^2-V}\right)^{-1}=\left(1-\frac{V}{2c^2}\right)^{-1}\sum_{k=0}^{\inf}\left(\frac{\epsilon}{V-2c^2}\right)^k \tag{2.18}$$

In practice it is not possible to include all the terms and in the most simple and most popular case, only the first term is taken into account. Since the first term had k=0 this is called the zeroth-order approximation (ZORA). The ZORA equation then reads:

$$\left(\frac{1}{2}(\boldsymbol{\sigma}\cdot\boldsymbol{p})\left(1-\frac{V}{2c^2}\right)^{-1}(\boldsymbol{\sigma}\cdot\boldsymbol{p})+V\right)\psi^L_{ZORA}(r)=\epsilon\psi^L_{ZORA}(r) \tag{2.19}$$

In calculations often spin-orbit interaction is not considered and the scalar relativistic ZORA equation reads:

$$\left(\frac{1}{2}\boldsymbol{p}\left(1-\frac{V}{2c^2}\right)^{-1}\boldsymbol{p}+V\right)\psi^L_{ZORA}(r)=\epsilon\psi^L_{ZORA}(r) \tag{2.20}$$

ZORA might be the simplest form of the regular approximation, but it can account for the most relevant relativistic effects and reproduces valence shell properties very well compared to fully relativistic four-component methods.

2.2.3 ECP

A completely different approach to including (scalar) relativistic effects is the use of effective core potentials. It is one of the oldest and most frequently used methods. Heavy atoms are split up in the valence electrons, which are chemically the most relevant, and the core. The core is removed from the explicit calculations by replacing it with an effective Hamiltonian. The fundamental approximations underlying the ECP method are the valence-core separation and the frozen core approximation. The use of ECPs allows for the inclusion of relativistic effects while also saving on computational cost as fewer electrons need to be included in the calculations. As ECPs are modelled on relativistic all-electron (AE) Hamiltonians, the accuracy of each ECP depends on the accuracy of the relativistic AE Hamiltonian [43].

2.3 Orbital Localization

Classical chemical concepts, such as bonds, valency, non-bonding electron pairs, are essential to practical chemistry. The formalism of quantum mechanics is fundamentally connected to the wavefunction, which is a non-local object, and not with more intuitive concepts such as

bonds. The many-electron wavefunction is an incredibly complex object, that can be built from molecular orbitals [44]. Canonical molecular orbitals (CMOs) are the eigenstates that correspond to the solutions of the self-consistent field (SCF) equations of Hartree-Fock (HF) or DFT theory. These CMOs are delocalized in space, but both HF and DFT theory are invariant under unitary transformations. This invariance gives the freedom to describe the system in terms of localised molecular(LMOs) without changing the final energy or electron density [45]. These LMOs correspond very well to the classical concepts such as bonds and are very useful in gaining better understanding of the system.

There are different methods to obtain the localized orbitals. In this section, only a posteriori methods are discussed, with a special focus on the Pipek-Mezey (PM) scheme as this is employed in this project. The methods discussed here are all used for localizing the occupied orbitals and not the virtual ones. For a more detailed discussion of the different methods, the reader is referred to [44]. There are different ways to obtain the LMOs from a set of CMOs, which usually involve the optimization of a certain functional. For the Foster-Boys scheme [46, 47] the spatial extent of the orbitals is minimized by minimizing the following functional:

$$L_{FB} = \sum_{k=x,y,z} \sum_{i \in occ} (\phi_i | r_k^2 | \phi_i \rangle - \phi_i | r_k | \phi_i \rangle^2) \tag{2.21}$$

The fourth moment (FM) [48] method is very similar to the FB method, only differing in taking the fourth moment instead of the second moment. It was introduced to obtain orbitals constricted to a small space but has the drawback of not being rotationally invariant [44]. The Edmiston-Ruedenberg localization [49] is based on maximizing the intraorbital coulomb repulsion:

$$L_{ER} = \sum_{i \in occ} \langle \phi_i \phi_i | \frac{1}{r_{\mu\nu}} | \phi_i \phi_i \rangle \tag{2.22}$$

Contrary to the FB method, this method preserves the separation of σ and π bonds, but due to higher computational cost the FB scheme is often preferred [50].

The most widely used localization scheme is the one introduced by Pipek and Mezey [51]. The PM scheme is based on atomic charges and does not mix σ and π bonds. It is based on maximizing the sum of the squared charges on each orbital:

$$L_{PM} = \sum_{atoms A} \sum_{i \in occ} [\langle \phi_i | P_A | \phi_i \rangle]^2 \tag{2.23}$$

Here P_A is the projection operator onto the atomic orbitals (AOs) centred on atom A. The partial charges used in the original PM scheme are Mulliken charges [52]. Mulliken charges arise from the Mulliken population analysis. In population analysis methods the electron density is expanded in terms of MOs, which in their turn can be expanded in terms of a set of atomic orbitals. This allows for the electron density to be written in the following form [53]:

$$\rho(r) = \sum_{\alpha\beta} D_{\alpha\beta} S_{\alpha\beta} \tag{2.24}$$

where $S_{\alpha\beta}$ is the overlap matrix between the atomic orbitals and $D_{\alpha\beta}$ the density matrix. Mulliken analysis is the most common used, but sometimes also called the worst population analysis [53]. In this method, half of the overlap population is assigned to each contribution orbital. Mulliken population analysis is mathematically quite ill-defined and highly dependent on the basis set used and there is no complete basis set limit [45]. These problems can be

overcome by generalizing the method and using atomic charges from methods that are better defined, as done by [45]. Another alternative is to obtain the partial charges by projection onto intrinsic atomic orbitals, as proposed by Knizia [54]. The major improvement of these intrinsic bonding orbitals (IBOs) is the removal of the basis set dependence while being of comparable computational costs.

2.4 X-ray Emission Spectroscopy

Where spectroscopy in the UV/vis range probes electronic transitions within the valence state, X-ray spectroscopy involves at least one core orbital. When valence states have very localized electron densities, making interpretation in terms of local changes difficult. The involvement of core orbitals in in X-ray spectroscopy provides the local probe of the electronic structure and since core-level energies are very element specific, X-ray spectroscopy is also element specific [55]. X-ray emission spectroscopy (XES) is an example of a photon-in/photon-out [56], were first the system in the ground state $|g\rangle$ is brought in an excited state $|n\rangle$ by the absorption of a photon. In the case of non-resonant XES, the core electron is excited to the continuum, so the state can be described as a photoionized state [17]. The excited state $|n\rangle$ then decays into a final state $|f\rangle$ by emission of a photon. Quantum mechanically this can be described by quantum mechanics using perturbation theory. The interaction between X-ray radiation and matter is briefly described below to give some background on the matter.

2.4.1 Theory of XES

The incoming X-ray photon can be described by the vector field $\mathbf{A}$. The interaction of this vector field with the sample can be described by an interaction Hamiltonian [57]:

$$H_{int} = \frac{e^2}{2m} \sum \boldsymbol{A}(\boldsymbol{r}_j)^2 + \frac{e}{m} \sum \boldsymbol{p}_j \cdot \boldsymbol{A}(\boldsymbol{r}_j) \tag{2.25}$$

Here $\mathbf{p}_j$ gives the momentum of the j-th electron. The term with $\boldsymbol{A}^2$ annihilates and creates a photon without the existence of an intermediate state. This accounts for Thomson, Raman and Compton scattering and is, with the exception of X-ray Raman spectroscopy, not relevant [57]. The cross-section part of the second term is proportional to the resonant Kramers-Heisenberg term [56]:

$$F_{KH}(\omega_{in}, \omega_{out}) = \frac{\omega_{out}}{\omega_{in}} \sum_f \left| \sum_n \frac{\langle f|O'^{\dagger}|n\rangle\langle n|O|g\rangle}{E_n - E_g - \hbar\omega_{in} - i\Gamma_n} \right|^2 \frac{\Gamma_f \ \pi}{(E_f - E_g - \hbar(\omega_{in} - \omega_{out})^2 + \Gamma_f^2} \tag{2.26}$$

Where O and O' represent operators involving the momentum of the electrons. Ignoring interference effects the equation can be simplified to [57]:

$$F_{KH}(\omega_{in}, \omega_{out}) = \frac{\omega_{out}}{\omega_{in}} \sum_f \sum_n \frac{|\langle f|O'^{\dagger}|n\rangle\langle n|O|g\rangle|^2}{(E_n - E_g - \hbar\omega_{in})^2 + \Gamma_n^2} \times \frac{\Gamma_f \ \pi}{(E_f - E_g - \hbar(\omega_{in} - \omega_{out})^2 + \Gamma_f^2} \tag{2.27}$$

About this equation some important points can be made with regards to X-ray spectroscopy :

- XES can always be described by the resonant KH term, independent of whether or not the incoming photon excites the electron to a unoccupied state or the continuum[56].
- for non-resonant XES, where there is an ionic intermediate and final state, the spectral broadening is independent of the incident energy bandwidth, making it possible to perform experiments with non-monochromatic radiation [58].

Another important note to make is that there are different ways to discuss the electronic transitions in complexes and molecules. There is the total energy picture, where the energy levels do not describe single electron levels, but total energy levels of the system. THe multi-electron picture is great for visualization of XES process where several electron levels are involved [59]. In chemistry electronic structures are described in terms of molecular orbitals and the transitions are simplified to one-electron transitions. This provides for a more intuitive way of describing the transition. Often even atomic orbitals instead of molecular orbitals are used to indicate the different energy levels [17, 56].

2.4.2 XES in the lab

As described, XES is based on a second-order process and is thus not restricted to synchrotron facilities, but can also be performed in a laboratory setting [60]. This can be very valuable as beam time at a synchrotron is highly competitive and not all experiments can be performed at such facilities. Experiments with complicated sample environments, long-time measurements, or study of materials with special safety procedures are examples of experiments that can often only be performed in a laboratory setting [10, 61]. Another advantage is that laboratory based X-ray experiments provide valuable learning experience when investigating new systems, which can result in more efficient use of beam time at synchrotron facilities. The major limitation for laboratory based experiments is the limited energies that can be achieved [10]

For XES there are four different type of geometries used to build high-energy resolution spectrometers. The transmission type spectrometer often uses a Laue-type DuMond geometry[62], while reflection type spectrometers are found with van Hámos[63], Johansson[64] or Johann[65] geometries. Each geometry has it's own advantages and disadvantages. The von Hámos spectrometer is based on a cylinderically bend analyser crystal, while both the Johansson and Johann spectrometers are based on spherically bend analyser crystals, see figure 2.1. For this thesis a x-ray spectrometer from the EasyXAFS brand is used, which uses a Johann geometry. For detailed information on the design and performance of such a spectrometer the reader is referred to [66].

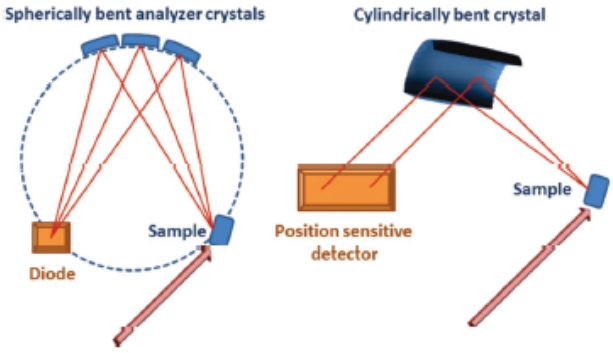

Figure 2.1: Schematic comparison of different spectrometer geometries. Image reprinted from [12].

3 Methods and Results

3.1 Computational Study

3.1.1 General Approach

All calculations were done using ORCA 4.2.1 [67, 68]. As the goal of this project is to investigate the possible improvement upon using relativistic methods compared to much cheaper composite methods such as B97-3c. The general procedure is to perform a geometry optimization and subsequently use the final geometry and CMOs to calculate the LMOs using the Pipek-Mezey scheme [51]. To do so, calculations are done using three levels of theory.

- **B97-3c** Firstly the B97-3c composite method [32] is used. This method is based on Becke's B97 GGA functional [69], with a modified def2-TZVP [70] basis set and corresponding ECP's [71] for heavier elements. Lastly two semi-classical correction potentials are added: the D3 London dispersion energy [30] and a short range basis (SRB) set correction energy [72]. Although the individual components that B97-3c is based on can also be used separately in ORCA, the B97-3c method also includes individual modifications [32].

- **B97-D3** To allow for a better investigation of the effect of using the ZORA method, calculations were also done using only methods that can also be combined with ZORA. It was tried to stay as close to the B97-3c method as possible. This second set of calculations are done using Grimme's B97-D3 functional [30, 73], which includes D3 London dispersion, the standard def2-TZVP [70] basis set and corresponding ECP's [71] and the RI approximation.

- **B97-D3 + ZORA** Lastly the same functional and basis set as before, but now using the ZORA method, which is an all-electron method, instead of using ECP's.

As described in 2.3, the PM localization scheme has the drawback of being basis on the ill-defined Mulliken charges. Knizia's IBO method [54] would therefore generally be a preferred option when calculating and comparing localized orbitals. This method is readily available both within ORCA and through Knizia's IboView program [54, 74]. However this method is based on the use of ECPs for heavier atoms and can not be used to perform orbital localization on the results from the all-electron ZORA calculations. This is why the PM method is employed to obtain the localized orbitals.

3.1.2 Geometry optimization

The geometry optimization was performed at each level of theory using the the *TightSCF Grid5 NoFinalGrid* settings in ORCA. Analytical frequency analysis on the optimized geometry confirmed that a true minimum was found. Unfortunately for complexes 2 and 4 the calculation at the ZORA level did not succeed after multiple tries. Due to time constraints, no optimized geometry was obtained. These complexes will therefore be excluded from the subsequent discussion on the orbital localization process. The effect of using the all-electron ZORA method over an ECP on the obtained geometries was judged using 3 different methods. Firstly the energies of each geometry evaluated at B97-D3 ZORA/def2-TZVP were compared by taking the energy difference with B97-D3 ZORA/def2-TZVP//B97-3c. Although comparing energies does not give all the information about a structure, it serves a good indication for how similar the

structures are. The results in figure 3.1 shows clearly that the largest deviation in energy comes from moving from the B97-3c method to the B97-D3 method. Those energy differences are still all under 1.4 kcal/mol, showing that there is still good agreement between the structures, with the clear exception of complexes 2 and 4 which show a larger difference. Upon including ZORA in the geometry optimization, energies of about 0.1 kcal/mol higher were obtained for all structures. This indicates that the difference in geometry that is obtained using ZORA is very small.

The second method to compare geometries is using the Root Mean Square Deviation (RMSD). Where for small highly symmetrical complexes geometries can easily be compared by comparing bond lengths, this is not a viable method for larger complexes. Using the RMSD the agreement between different geometries, no matter their complexity, can be expressed as one number. For this a python script by Kromann [75] was used. Here the RMSD is minimized by translation and rotation of the two molecules using the Kabsch algorithm [76]. The results of comparison of the full geometries can be found in figure 3.2. Complexes 2 and 4 show large values, indicating that the geometries obtained using B97-3c and B97-D3 do not agree well with each other. Removing those outliers (figure 3.3 allows for a closer look at the RMSD of the other complexes. In general those structures all agree very well with each other. For reference the RMSD value between B97-3c and B97-D3 for complex 9 ($AuBr_4^{-1}$) is 0.0117 and the difference in Au-Br bond length for those two geometries is 0.01 Å. This can be considered a very good agreement. With the exception of comples 5 ($AuCl_4^{-1}$) the best agreement is found between B97-D3 and B97-D3 ZORA.

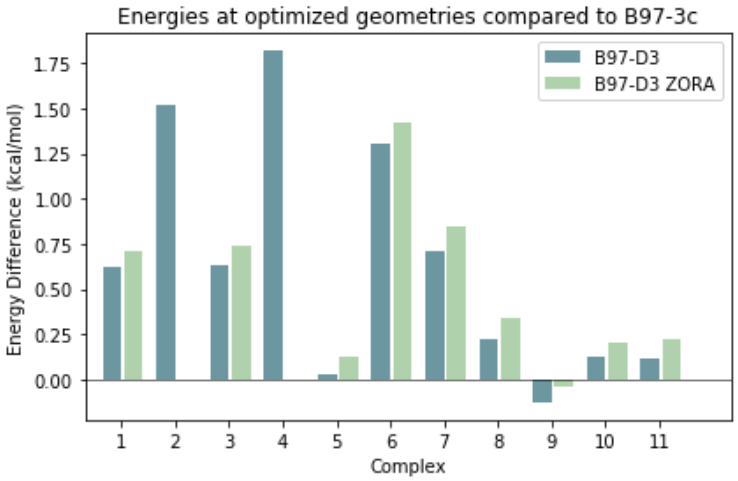

Figure 3.1: Energy differences in single point calculations at the B97-D3 ZORA level of theory on the geometry at the B97-3c level and single point calculations at the B97-D3 ZORA level on the geometries obtained using B97-D3 and B97-D3 ZORA.

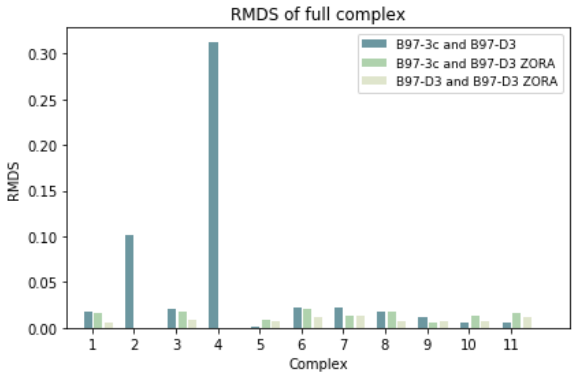

Figure 3.2: RMSD values for the geometries obtained at different levels of theory

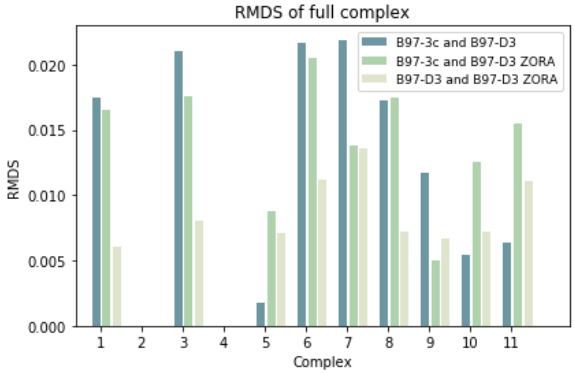

Figure 3.3: RMSD values for the geometries obtained at different levels of theory, excluding complexes 2 and 4.

When taking the full complex into account when comparing the geometries, either by calculating the energies or by taking the RMSD, difference become larger when the molecule has more atoms and less symmetry. This explains the clear difference between the complexes with large organic ligands and the complexes with only halides atoms (AuF_4^{-1}, $AuCl_4^{-1}$, $AuBr_4^{-1}$, $AuCl_3$). As for this thesis the bonds between the gold atom and the ligands are of the most interest as the first coordination sphere is the most important for reactivity, the RMSD was also calculated using only the positions of those atoms. Using this method (figure 3.4) a clear decrease in the RMSD value can be found, indicating that the positions of the atoms bonded to the gold does not change significantly using the different levels of theory. Now the earlier seen trend of the difference between B97-D3 and B97-D3 ZORA being the smallest also no longer holds true. A possible explanation for this is that for those two methods the results for the lighter atoms in the ligands, where relativistic effects are less, behaved very similarly, while for the B97-3c the effects of the augmentations implemented by Grimme and coworkers [32] are more more pronounced.

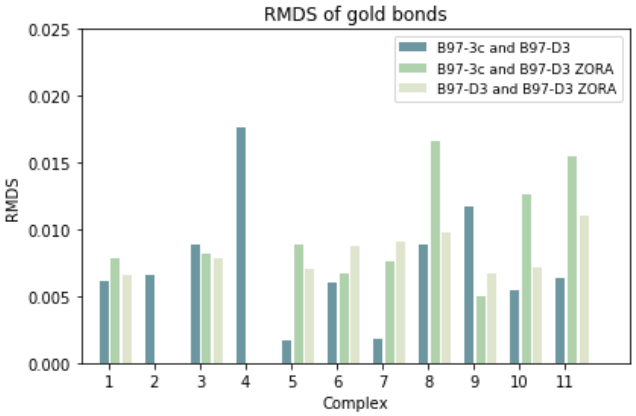

Figure 3.4: RMSD values only taking into account the atoms involved in bonds or coordination to gold.

Combining all three ways to compare the geometries it can be concluded that the moving from an ECP based method to method that includes ZORA will give some differences in the geometries, but those are of a similar order as or smaller than the difference in when changing from B97-3c to B97-D3. In general all three methods yield geometries that agree very well with each other, making the use of ZORA in geometry optimizations not very favourable considering the higher computational costs. What the effect of these small differences is on the electronic structure and orbital localization is investigated at the end of the next section.

3.1.3 Orbital Localization

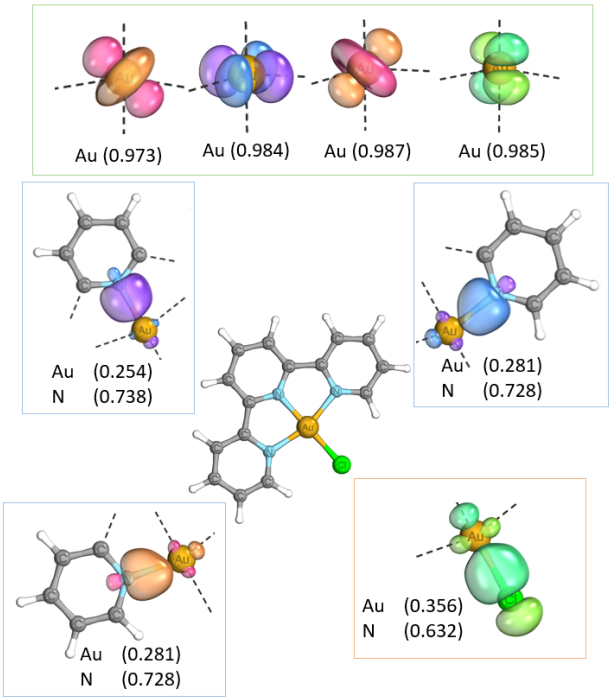

Figure 3.5: Localized bond orbital depictions of the occupied d-orbitals (top) and the Au-ligand bonding orbitals for complex 1, (2,2',2"-terpydrine)gold(III)chloride.

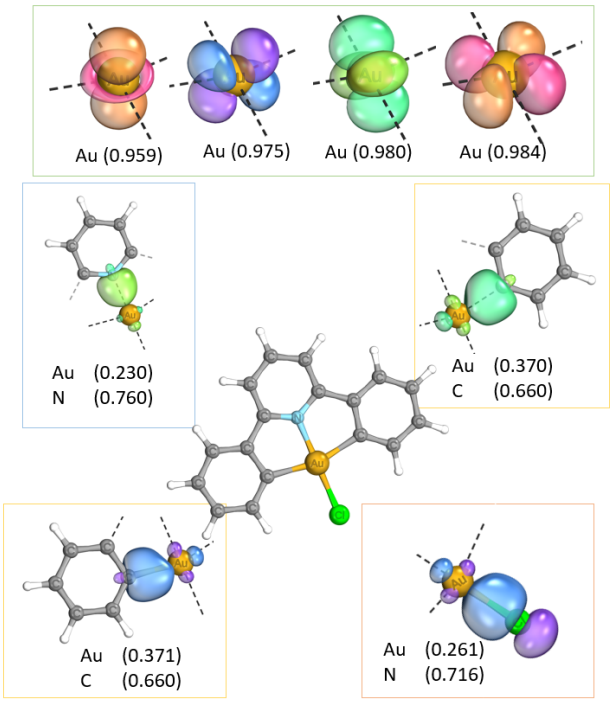

Figure 3.6: Localized bond orbital depictions of the occupied d-orbitals (top) and the Au-ligand bonding orbitals for complex 3, (2,6-Diphenylpyridine)gold(III)chloride.

The orbital localization was performed using the PM scheme at the same level of theory as the geometry optimizations are done. For each of the localized orbitals involved in the bonding to the gold the coefficients on each the atoms between which the bond is formed are extracted. These coefficients are taken as a measure of how electron-sharing a bond is. Here a coefficient of 1 indicates that the orbital fully resides on one atom, while a coefficient of 0.5 on each atom would indicate perfect sharing of the electrons between the atoms. So for example the values close to 1 for the d-orbitals in figure 3.5 indicate that the doubly occupied orbital (almost) fully resides on the gold atom. In this sections the localized orbitals are visualized using IboView for the B97-D3 ZORA calculations. Orbital iso-surfaces enclose 80% of the integrated electron density of the orbital. All orbitals are doubly occupied.

For complex 1, (2,2',2"-terpydrine)gold(III)chloride, and complex 3, (2,6-Diphenylpyridine) gold(III)chloride, the four doubly occupied d-orbitals correspond well to the d8 configuration associated with the formal +3 oxidation state. However a closer look at the orbital coefficients of the bond orbitals reveal a somewhat covalent character, which causes a higher effective charge on the gold atom. The bonds are still polarized towards the ligand. The C-Au bond in complex 3 has a more covalent character than the Au-N bonds in complexes 1 and 3, which agrees well with the electronegativity of the respective atoms. From table 3.1 it can be seen that upon changing to the ZORA method the Au-C and Au-N bonds become more covalent in nature, while the Au-Cl bond becomes more polarized.

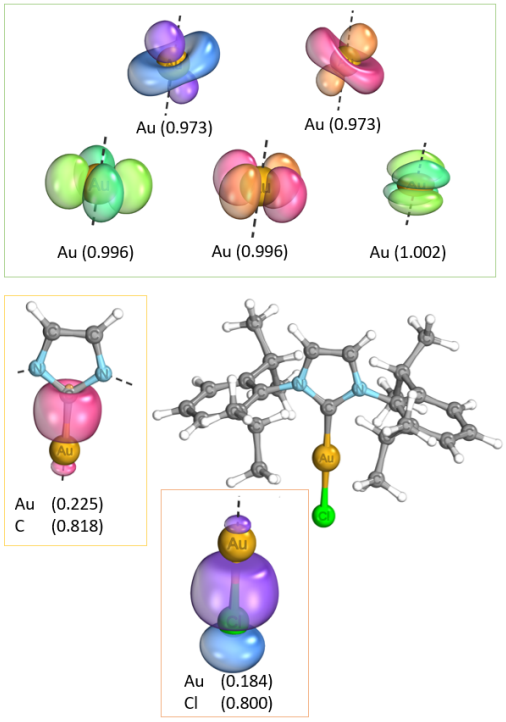

Figure 3.7: Localized bond orbital depictions of the occupied d-orbitals (top) and the Au-ligand bonding orbitals for complex 6, (1,3-Bis(2,6-diisopropylphenyl)-1H-imidazol-3-ium))gold(I)chloride.

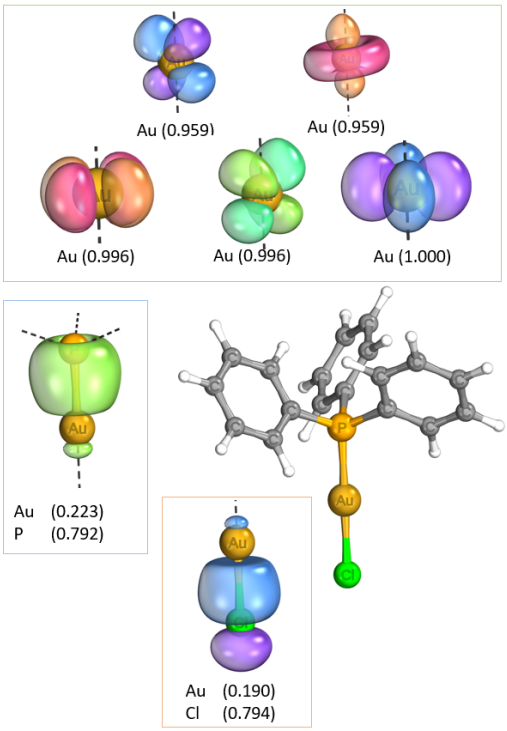

Figure 3.8: Localized bond orbital depictions of the occupied d-orbitals (top) and the Au-ligand bonding orbitals for complex 7, Ph_3PAuCl.

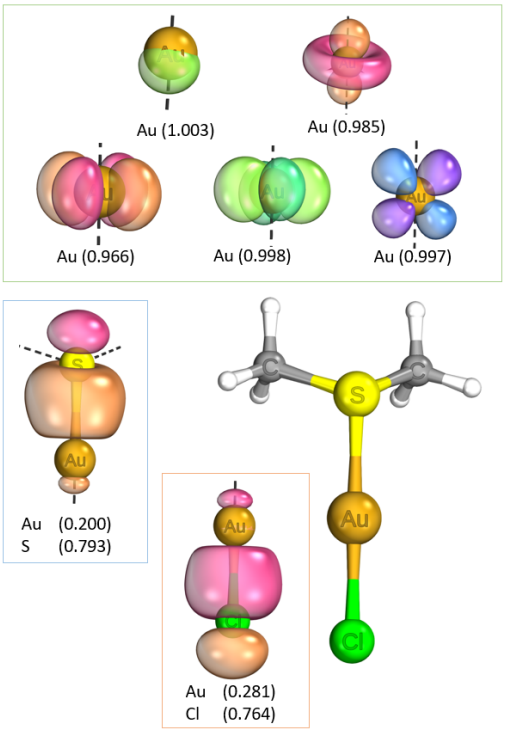

Figure 3.9: Localized bond orbital depictions of the occupied d-orbitals (top) and the Au-ligand bonding orbitals for complex 8, DMSAuCl.

For the three complexes with a formal oxidation state of +1, there are 5 doubly occupied d-orbitals, as is expected (d10 configuration). For complex 6, 1,3-Bis(2,6-diisopropylphenyl)-1H-imidazol-3-ium))gold(I)chloride, and complex 8, DMSAuCl, the shapes of the d-orbitals do not correspond to the expected shapes.For complex 6 the top two orbitals both show somewhat of a combination of the doughnut and four lobe shape. This can be due to the visualization of 80% of the isosurface, as they both still show the symmetry expected for a d-orbital. For complex 8 the first orbital can not be related to any of the traditional shapes of d-orbitals and does not show the symmetry related to d-orbitals. It is possible that this is an indication that the orbital localization was not completely succesful. The general trend for these complexes is that the gold-ligand bonds have a less covalent character than for complexes 1 and 3. Similar to previously the Au-Cl bonds become more polarized when using ZORA, while the Au-C bond becomes less polarized. The Au-P and Au-S bond also show this effect, but to a lesser extent. For the B97-3c calculation on complex 7, the bonding orbital of the Au-P bond could not be identified. It is suspected that this bond has a strongly dative character and is

a such not recognized by the program as a bond-like orbital. For $[AuBr_4]^{-1}$, $[AuCl_4]^{-1}$ and $[AuF_4]^{-1}$ a clear trend is visible that when going down the periodic table the bond gets less polar. For these more simple complexes, as well as for $AuCl_3$ the population coefficients change the least when changing methods.

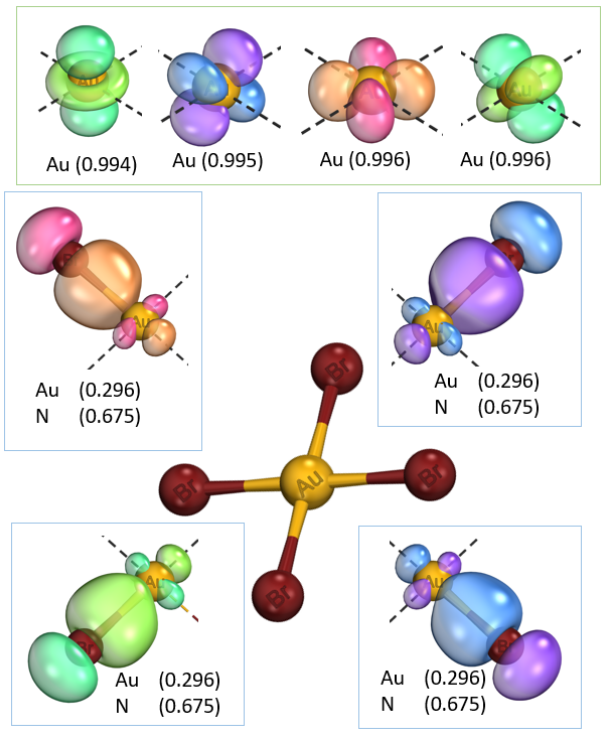

Figure 3.10: Localized bond orbital depictions of the occupied d-orbitals (top) and the Au-ligand bonding orbitals for complex 9, $AuBr_4^{-1}$.

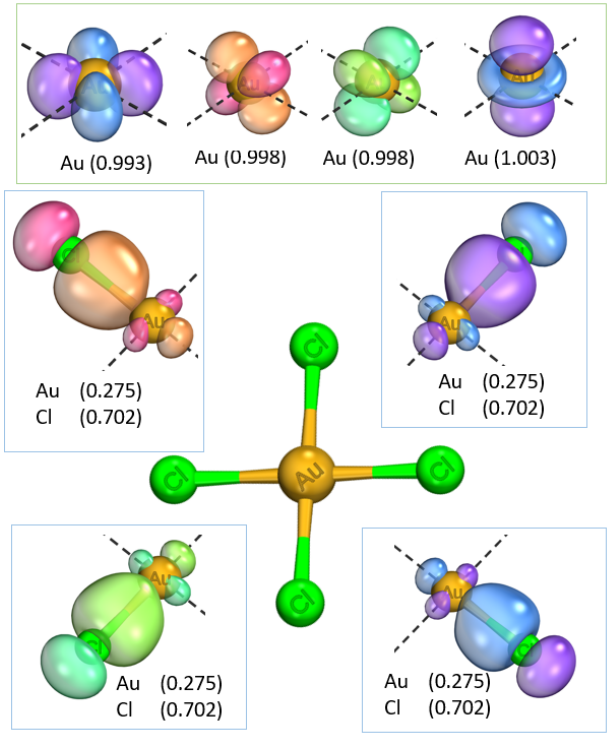

Figure 3.11: Localized bond orbital depictions of the occupied d-orbitals (top) and the Au-ligand bonding orbitals for complex 5, $AuCl_4^{-1}$.

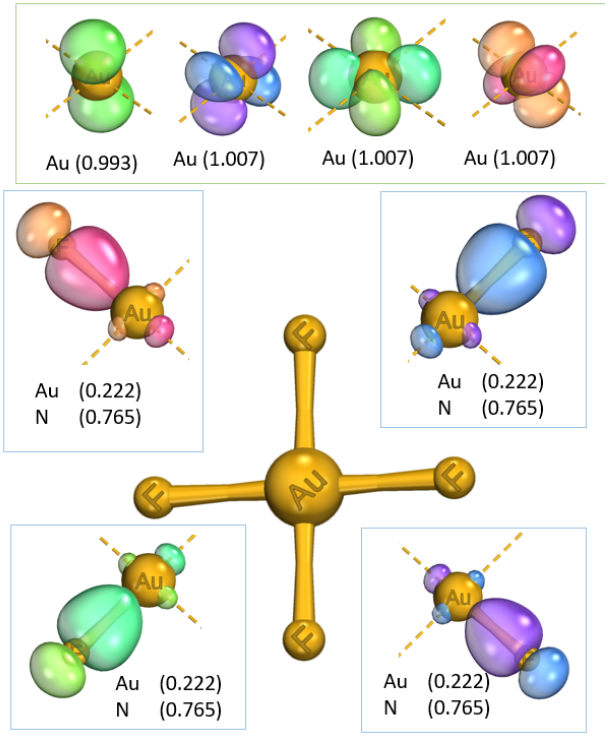

Figure 3.12: Localized bond orbital depictions of the occupied d-orbitals (top) and the Au-ligand bonding orbitals for complex 10, AuF_4^{-1}.

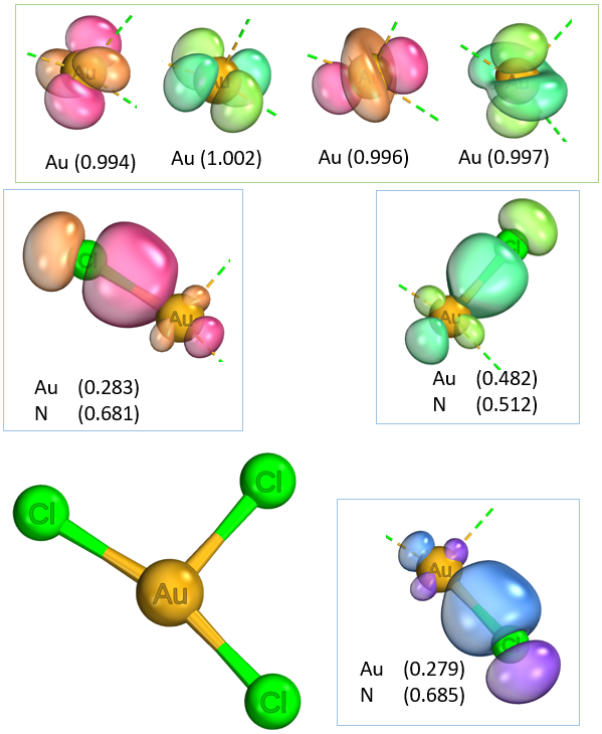

Figure 3.13: Localized bond orbital depictions of the occupied d-orbitals (top) and the Au-ligand bonding orbitals for complex 11, $AuCl_3$.

From all the localized orbitals it is clear that each of the ligands provides some charge to the gold atom. This effect seems to be more pronounced in the complexes with a formal oxidation state of 3+. As expected for a PM localization scheme the population coefficients are strongly dependent on the method used. A general trend can be found that when an all-electron scalar relativistic method is used instead of an ECP. The Au-X bond, where X = F, Cl, Br, has less or an equal charge residing on the gold, while the Au-ligand bonds shows a higher population coefficient on the gold. It was confirmed that these changes are not due to the change in geometry alone by performing the localization procedure at the B97-D3 ZORA level of theory on each of the optimized geometries. Those results showed very similar coefficients for each geometry, see Appendix A, showing that the effect is clearly due to using ZORA at the localization step.

3.2 XES

3.2.1 Apparatus and Sample Preparation

Laboratory-based XES measurements were performed using the easyXES100 spectrometer [77]. The easyXES100 is equipped with a Vortex VF80-JM x-ray tube and a Silicon Drift Detector (SDD). A Si(933) crystal was used as the focus of this experiment is on the Lβ_5 (5d to 2p) valence to core transition, which is reported to be around 11914 eV for Au [78, 79]. As this line is very weak, the Lβ_3 (3p to 2s) line at 11610 eV [78, 79] is used to calibrate. The offset as well as the optimal sample position were determined with a gold foil sample. Samples of complexes 3, 7, 8, 9 and 11 were prepared by taking 3-6 mg of each sample and packing it onto the sample holder without mixing it with any substance to dilute it. The sample was sealed using scotch tape. The sample was placed as close to the x-ray tube as possible on the Rowland circle and

Atom	Population coefficients			Atom	Population coefficients		
	B97-3c	B97-D3	ZORA[a]		B97-3c	B97-D3	ZORA[a]
Complex 1							
Au	0.266	0.288	0.281	N	0.725	0.735	0.728
Au	0.266	0.288	0.281	N	0.725	0.735	0.728
Au	0.140	0.184	0.254	N	0.833	0.824	0.738
Au	0.438	0.387	0.356	Cl	0.590	0.640	0.632
Complex 3							
Au	0.186	0.237	0.230	N	0.829	0.776	0.760
Au	0.329	0.328	0.371	C	0.903	0.853	0.660
Au	0.329	0.328	0.370	C	0.903	0.853	0.660
Au	0.380	0.320	0.261	Cl	0.653	0.720	0.716
Complex 6							
Au	0.112	0.151	0.225	C	0.930	0.919	0.818
Au	0.258	0.221	0.184	Cl	0.765	0.789	0.800
Complex 7							
Au		0.217	0.223	P		0.759	0.792
Au	0.271	0.237	0.190	Cl	0.755	0.777	0.794
Complex 8							
Au	0.199	0.198	0.200	S	0.811	0.797	0.793
Au	0.267	0.254	0.231	Cl	0.743	0.753	0.764
Complex 9 [b]							
Au	0.295	0.290	0.296	Br	0.682	0.688	0.675
Complex 5 [b]							
Au	0.280	0.270	0.275	Cl	0.702	0.712	0.702
Complex 10 [b]							
Au	0.221	0.223	0.222	F	0.771	0.769	0.765
Complex 11							
Au	0.489	0.482	0.482	Cl	0.508	0.516	0.512
Au	0.286	0.277	0.283	Cl	0.677	0.686	0.681
Au	0.286	0.277	0.279	Cl	0.677	0.687	0.685

Table 3.1: Population coefficients of localized orbitals for all complexes. Any values that stand out are marked in red. [a] *B97-D3 ZORA is abbreviated as ZORA.* [b] *For these complexes one the coefficient for one bonding orbital is given, as all bonding orbitals are equal due to symmetry.*

care was taken to make sure the sample was placed in the same position every time. Due to the sensitivity of the spectrometer to minor changes in the angle, the sample holder was slightly rotated every time to find the largest Lβ_3 signal. For each sample multiple scans were done over a period of around 2 hours. Details on the scan rate, offset and energy zones can be found in appendix B.

3.2.2 XES measurements

The results from the XES measurements are summarized in in figure 3.14. For all data the Lβ_3 transition is found to be 11586 eV, which is different from the reported value for elemental gold of 11610 eV by 24 eV for all samples. The Lβ_5 peak however is positioned at the expected energy of 11915 eV. The peak at 11586 eV shows two possible shoulders. The first one at approximately 11566 eV can be attributed to the Lβ_2 line of gold. The shoulder at the higher energy could not be easily assigned. For the HAuBr4 sample no Lβ_5 was observed. Two strong peaks at 11924 eV and 11878 eV are assigned to the Kα_1 and Kα_2 transitions of bromine, corresponding in energy and relative intensities [78, 79]. For this sample the Lβ_5 peak of the gold is expected to be within the shoulder of the bromine Kα_1 peak and can thus not be observed. All other samples showed the Lβ_5 peak at the same position as efor the gold foil. No distinction could be made between complexes with different ligands or different formal oxidation states based on peak position, although there is a slight difference in shape of the peaks visible. This is in line with the results reported by Castillo et al [1] for the Kβ mainlines for 3d transition metal complexes showing either no energy shifts at all on less than 0.3 eV. This can possibly be attributed to the canceling effects of covalency and change in d-count [1, 80]. This could connect to the covalent character of the localized bond orbitals in complexes 1 and 3, compared to complexes 6, 7, and 8. Relative peak intensities were compared by taking the peak area, as summarized in table 3.2. There seems to be some trend correlating the formal oxidation state to the ratio, but this is not conclusive as the the difference between $AuCl_3$ and 3 is as large as the difference with complexes with formal oxidation states of +1. This data is even more difficult to interpret due to the questions about the stability of some of the samples, as discussed later on.

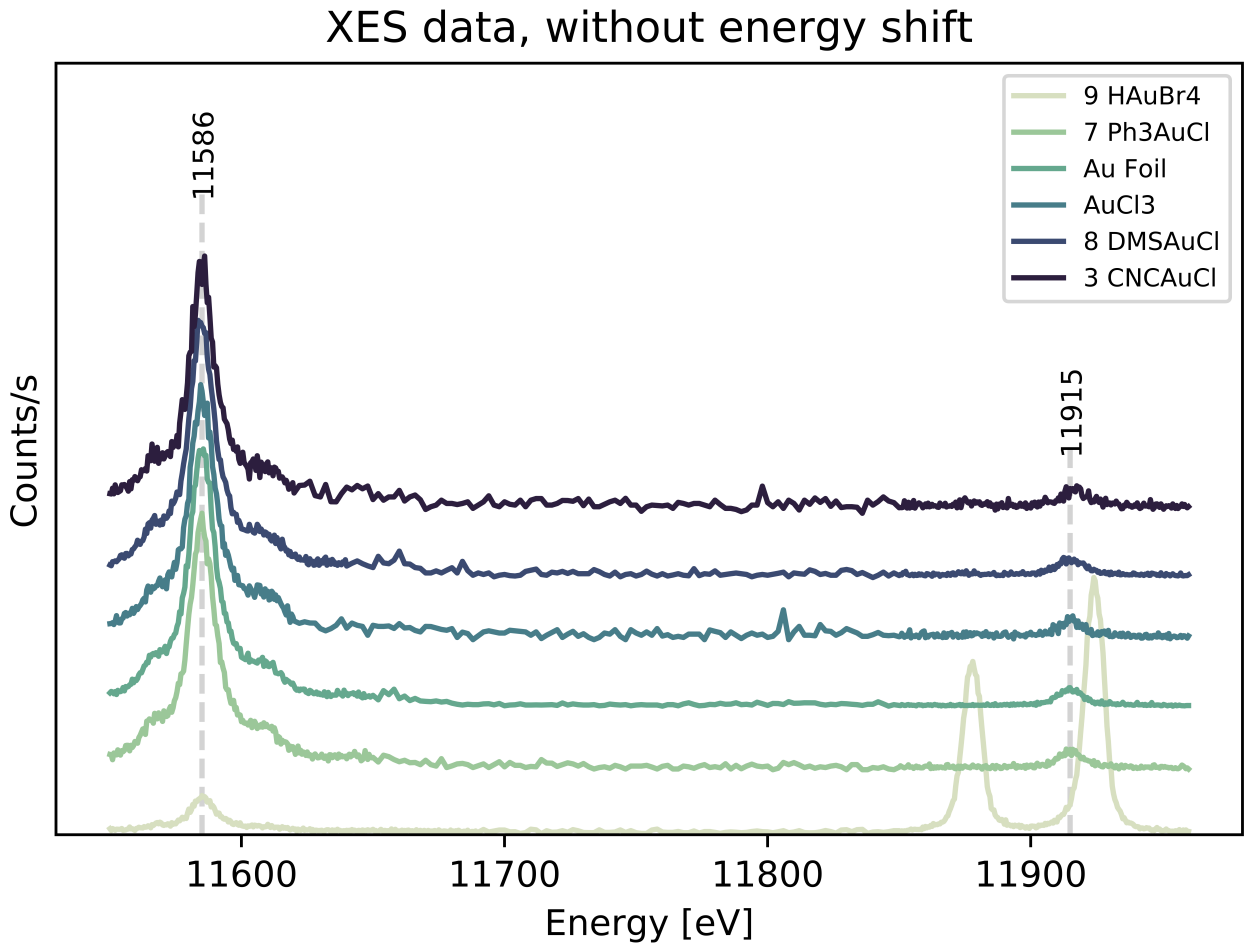

Figure 3.14: XES data, where CNC stands for the tridentate 2,6-Diphenylpyridine ligand

3.2.3 Stability of samples

As each measurement was performed over a period of 2 hours and at room temperature, the samples were checked for decomposition. For $HAuBr_4$ Raman spectra taken before and after the measurement showed no signs of decomposition, and a peak at 422 $cm^{-}1$ characteristic for the Au-Br bond. Complex 7, Ph_3AuCl, the sample was accidentally cleaned before spectra could be taken. To test the stability a new sample was prepared and left in air for the duration of the measurement to simulate the conditions. Both ^{1}H-NMR and ^{31}P-NMR spectra before (as provided by the Klein group) and after showed the sample in high purity and without any signs of decomposition. The Raman spectra confirmed this. The Raman spectra show good agreement with the theoretical spectra obtained at the B97-3c level after scaling with linear regression. Complex 3, 2,6-(Diphenylpyridine)gold(III)chloride, showed no signs of decomposition on ^{1}H-NMR. Due to time constraints a Raman spectrum could only be obtained before the measurement, but not after. Although the spectrum showed some sig-

Sample	Formal OS	Area Lβ_3	Area Lβ_5	Ratio
Au Foil	0	3853	197.6	0.051
Ph3AuCl	I	1897	122.1	0.064
DMSAuCl	I	1852	116.2	0.063
AuCl3	III	916.4	69.01	0.075
CNCAuCl	III	840	77.02	0.092

Table 3.2: Ratios of the peaks as determined by peak area.

nificant fluorescence, major peaks agreed well with the computed spectrum after a baseline correction. For complex 8, DMSAuCl, a change in colour from beige grey to a more blueish grey was observed. Both ^{1}H-NMR and Raman spectra after the measurement showed no trace of the original complex. This is in line with the compound being know do decompose quickly in air [81]. The Raman spectrum taken before the measurement, does not agree with reported Raman spectra [82] and the computed spectrum. It is therefore possible that decomposition already started. Of $AuCl_3$ no Raman or NMR spectra were taken as this would not yield any useful information. All NMR spectra of the complexes can be found in Appendix C.

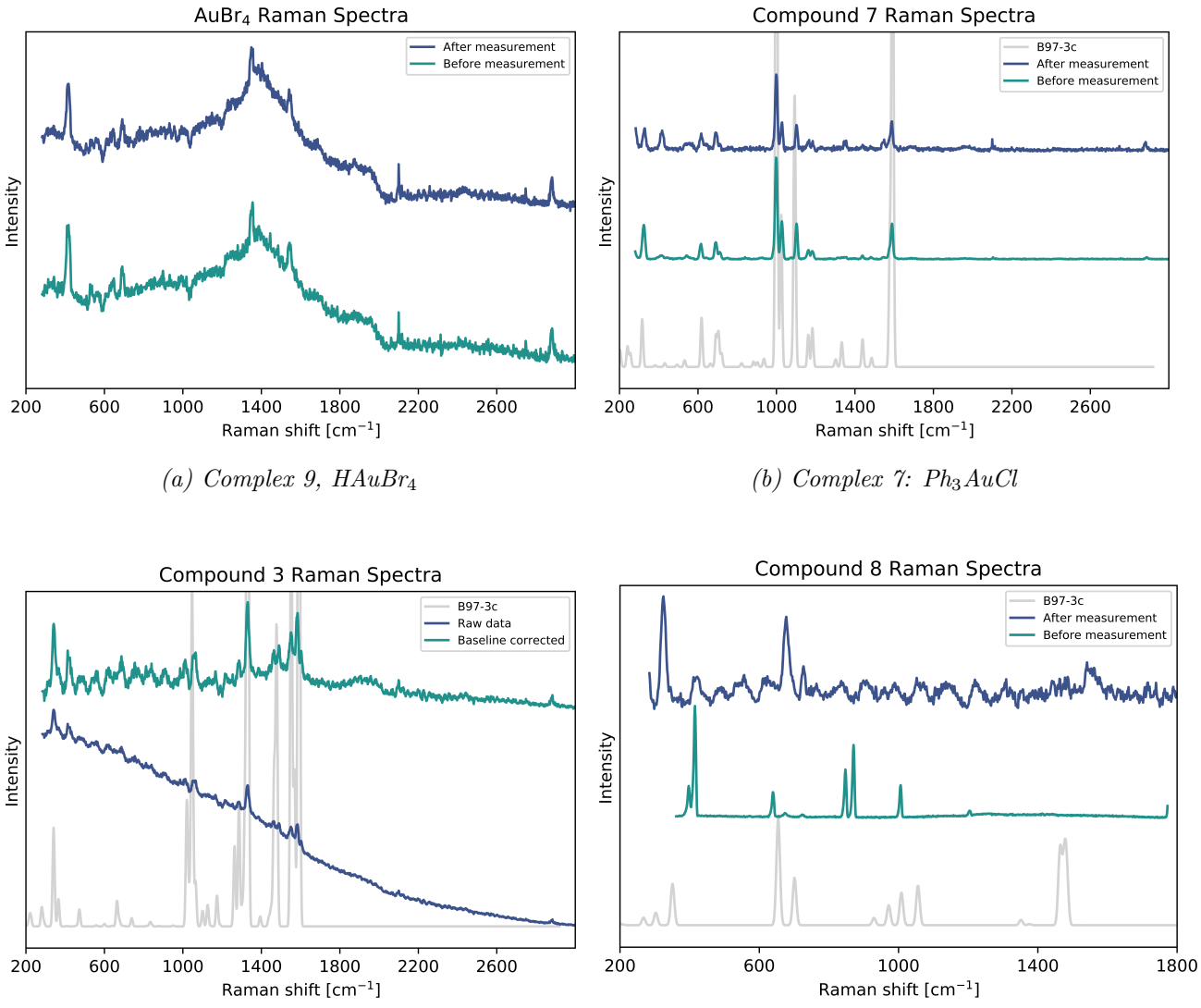

(a) Complex 9, $HAuBr_4$

(b) Complex 7: Ph_3AuCl

(c) Complex 3, (2,6-Diphenylpyridine)gold(III)chloride

(d) Complex 8, DMSAuC

Figure 3.15: Raman spectra of complexes taken before and after XES measurement. When applicable the spectra are compared against the simulated spectra (B97-3c)

4 Discussion

In this section, remarks are made on both the accuracy and applicability of the computational results and the experimental results. Suggestions on further exploration of these results are also given. The accuracy in computational methods can be described in terms of physical accuracy, that is how well does the system describe the real system, and the numerical accuracy, how well does the system converge. The main source in DFT calculations is the use of an approximate functional to describe the exchange-correlation effects. In this thesis functionals were used that are not optimized for transition metal complexes, which might introduce some inaccuracies, especially for the B97-3c functional, as this functional makes use of individual modifications to the basis set and dispersion corrections [32]. The way scalar relativistic effects are implemented are, as described in the theory, a source of error. These are errors that need to be kept in mind, but are not necessary parts than can be easily improved on. For the orbital localization method there are some points to be improved upon. As the Pipek-Mezey localization scheme depends on Mulliken population analysis, it is very difficult to separate the influence of the method on the mulliken population analysis from the influence of the all electron relativistic ZORA method on the effective partial charges on the gold atom. The sometimes off looking shapes of the d-orbitals are also an indication that the localization was not optimal. It would be interesting to see what the results would be if there is a way to perform the orbital localization for all electron system by projection on a minimal basis set, similar to the IBO's of Knizia [54, 74].

Looking at the numerical accuracy the notion of basis set truncation should be made. Another point related to numerical accuracy is the possibility that a local minimum is found instead of a global minimum due to the iterative nature of the calculations. For heavier elements, such as the gold atom in the calculations performed, the angluar grid used in the calculations can also influence the calculations. Manual exploration of the grid dependence for these transition metal complexes might be needed [83]. Further investigation could also include continuing the geometry optimization of complexes 2 and 4. This might be especially interesting considering the larger differences in the geometries from the B97-3c and B97-D3 methods.

Related to the experimental results, no difference in the peak position of the Lβ5 peak was found for the selected gold complexes. However, since this peak is quite weak in the spectra taken, longer measurements could provided a better signal to noise ratio. This could be especially interesting with regard to the relative intensity of the peaks, as some differences were found, but there is not enough data to really draw any conclusions from this. Based on the computational results there should be a difference in the electron density on the gold atom and it would be expected that this would translate in differences in intensities of certain peaks. Furthermore the influence of different ligands was expected to be larger, as XES has been used successfully to distinguish different ligands and different oxidation states [1, 12, 14]. It should be noted that to do so, the stability of some of the samples should be investigated more thoroughly, as especially complex 8 seemed to decompose. A possibly interesting next step would be to perform XES at lower temperatures, to see if that has effect on the stability of the samples. Another point of discussion it the position of the Lβ3 peak being at 11586 eV, which is 24 eV from the literature value of 11610 eV [78, 79]. This difference could be due to inaccuracies during the calibration of the X-ray spectrometer.It should also be considered that the literature values are obtained at a synchrotron, so using a single excitation energy, while in the lab a broader energy range is used.

5 Conclusion

In this thesis several different gold complexes were investigated using both XES and computational methods in order to gain better understanding in the electronic structure of gold complexes with different formal oxidation states. 11 complexes with formal oxidation states of +1 and +3 and various different ligands were selected.

Laboratory based XES measurements on the Lβ_5 and Lβ_3 transition were done for 5 of the complexes using the EasyXES100 spectrometer with gold foil as a reference. No significant shift in position of the Lβ_5 and Lβ_3 peaks was found for any of the samples. For the $HAuBr_4$ sample no Lβ_5 was observed as it coincides with the much stronger Kα_1 peak of the bromine. No distinction could be made between complexes with different ligands or different formal oxidation states based on peak position. Comparing the relative peak intensities of the Lβ_5 peak showed some indication of a trend, but this was not conclusive.

The computational part of this study was focused on two main questions. The first question is about the differences between using the composite B97-3c method and the all electron ZORA method for both geometry optimization as well as orbital localization. To also be able to see the direct effect of using the ZORA method, the B97-D3 functional and an appropriate ECP was used to closely mimic the B97-3c method, as the B97-3c method can not be combined with ZORA. Using different methods to compare the geometries it was found that going from the B97-3c to the B97-D3 method generally showed larger changes then going from the B97-D3 method to the B97-D3 method with ZORA. Comparison of the single point energies showed that the energies were consistently around 0.1 kcal/mol higher when using the ZORA method. RMSD between the different geometries showed very good agreement between the different methods, both when considering the full complex as well as when only the first coordination sphere is considered. In general all three methods yield geometries that agree very well with each other, making the use of ZORA in geometry optimizations not very favourable considering the higher computational costs. For the orbital localization a significant difference was found when changing to the all-electron ZORA calculations. A general trend can be found that when an all-electron scalar relativistic method is used instead of an ECP. The Au-X bond, where X = F, Cl, Br,has less or an equal charge residing on the gold, while the Au-ligand bonds shows a higher population coefficient on the gold. This indicates that there could be a benefit of using ZORA instead of ECP's when performing orbital localization, although it should be mentioned that the PM scheme is higher dependent on the method used, so this could also be the main cause of the differences. The second question is about how the orbital localization can give better insight in the differences in electronic structure between complexes with different formal oxidation states. From all the localized orbitals it is clear that each of the ligands provides some charge to the gold atom, with this effect being more pronounced for complexes with a higher formal oxidation state. This cancelling effect of covalency could possibly relate to why no changes the energy of the Lβ_5 peak was found.

Further computational and experimental work can be conducted in the following area's. Computationally it would be interesting compare the results of different localization methods, especially methods that are less dependent on basis set, such as the IBO method. Including a larger range of complexes, possibly also with other 5d elements could be useful for finding any more general trends. To better be able to predict and relate the changes seen in the electronic structure to X-ray spectroscopy ground state could be used to simulate the XES

spectra and evaluate contributions to energies and intensities. Experimentally it apart from the Lβ_5 transition, other valence-to-core transitions could be investigated. Especially interesting could be any transitions of the ns or np state of the ligand to the a core orbital of the electron, as these transitions could be even more sensitive to the ligand and oxidation state.

Bibliography

[1] R.G. Castillo, A.W. Hahn, B.E. Van Kuiken, J.T. Henthorn, J. McGale, and S. DeBeer. Probing physical oxidation state by resonant x-ray emission spectroscopy: Applications to iron model complexes and nitrogenase. *Angewandte Chemie*, 133(18):10200–10209, 2021.

[2] F. Wöhler. *Grundriss der chemie*. Duncker und Humblot, 1854.

[3] M. Jansen and U. Wedig. A piece of the picture—misunderstanding of chemical concepts. *Angewandte Chemie International Edition*, 47(52):10026–10029, 2008.

[4] H. Raebiger, S. Lany, and A. Zunger. Charge self-regulation upon changing the oxidation state of transition metals in insulators. *Nature*, 453(7196):763–766, 2008.

[5] R. Resta. Charge states in transition. *Nature*, 453(7196):735–735, 2008.

[6] P. Karen, P. McArdle, and J. Takats. Toward a comprehensive definition of oxidation state (iupac technical report). *Pure and Applied Chemistry*, 86(6):1017–1081, 2014.

[7] V. Postils Ribó, C. Delgado Alonso, J.M. Luis Luis, and P. Salvador Sedano. An objective alternative to iupacqs approach to assign oxidation states. *© Angewandte Chemie International Edition, 2018, vol. 57, núm. 33, p. 10525-10529*, 2018.

[8] J.S. Steen, G. Knizia, and J.E.M.N. Klein. σ-noninnocence: Masked phenyl-cation transfer at formal niiv. *Angewandte Chemie*, 131(37):13267–13273, 2019.

[9] P. Chaudhuri, C.N. Verani, E. Bill, E. Bothe, T. Weyhermüller, and K. Wieghardt. Electronic structure of bis (o-iminobenzosemiquinonato) metal complexes (cu, ni, pd). the art of establishing physical oxidation states in transition-metal complexes containing radical ligands. *Journal of the American Chemical Society*, 123(10):2213–2223, 2001.

[10] P. Zimmermann, S. Peredkov, P.M. Abdala, S. DeBeer, M. Tromp, C.h Müller, and J.A. van Bokhoven. Modern x-ray spectroscopy: Xas and xes in the laboratory. *Coordination Chemistry Reviews*, 423:213466, 2020.

[11] P. Glatzel and U. Bergmann. High resolution 1s core hole x-ray spectroscopy in 3d transition metal complexes—electronic and structural information. *Coordination chemistry reviews*, 249(1-2):65–95, 2005.

[12] M. Bauer. Herfd-xas and valence-to-core-xes: new tools to push the limits in research with hard x-rays? *Physical Chemistry Chemical Physics*, 16(27):13827–13837, 2014.

[13] N. Lee, T. Petrenko, U. Bergmann, F. Neese, and S. DeBeer. Probing valence orbital composition with iron kβ x-ray emission spectroscopy. *Journal of the American Chemical Society*, 132(28):9715–9727, 2010.

[14] R. Ravel, A.J. Kropf, D. Yang, M. Wang, M. Topsakal, D. Lu, M.C. Stennett, and N.C. Hyatt. Nonresonant valence-to-core x-ray emission spectroscopy of niobium. *Physical Review B*, 97(12):125139, 2018.

[15] C.J. Doonan, L. Zhang, C.G. Young, S.J. George, A. Deb, U. Bergmann, G.N. George, and S.P. Cramer. High-resolution x-ray emission spectroscopy of molybdenum compounds. *Inorganic chemistry*, 44(8):2579–2581, 2005.

[16] V.V. Pryadchenko, V.V. Srabionyan, L.A. Avakyan, J.A. van Bokhoven, and L.A. Bugaev. Electronic structure of pt and au compounds measured by x-ray emission and x-ray absorption spectroscopies. *The Journal of Physical Chemistry C*, 116(49):25790–25796, 2012.

[17] E. Gallo and P. Glatzel. Valence to core x-ray emission spectroscopy. *Advanced Materials*, 26(46):7730–7746, 2014.

[18] S. DeBeer George and F. Neese. Calibration of scalar relativistic density functional theory for the calculation of sulfur k-edge x-ray absorption spectra. *Inorganic chemistry*, 49(4):1849–1853, 2010.

[19] C. van Wüllen. Relativistic density functional theory. In *Relativistic methods for chemists*, pages 191–214. Springer, 2010.

[20] P.W. Atkins and R.S. Friedman. *Molecular quantum mechanics*. Oxford university press, 2011.

[21] D. Sholl and J.A. Steckel. *Density functional theory: a practical introduction*. John Wiley & Sons, 2009.

[22] H. Jacobsen and L. Cavallo. Directions for use of density functional theory: A short instruction manual for chemists. Springer Nature, 2017.

[23] P. Hohenberg and W. Kohn. Inhomogeneous electron gas. *Physical review*, 136(3B):B864, 1964.

[24] W. Kohn and L.J. Sham. Self-consistent equations including exchange and correlation effects. *Physical review*, 140(4A):A1133, 1965.

[25] J.D. Watts, J. Gauss, and R.J. Bartlett. Open-shell analytical energy gradients for triple excitation many-body, coupled-cluster methods: Mbpt (4), ccsd+ t (ccsd), ccsd (t), and qcisd (t). *Chemical physics letters*, 200(1-2):1–7, 1992.

[26] L. Goerigk and N. Mehta. A trip to the density functional theory zoo: warnings and recommendations for the user. *Australian Journal of Chemistry*, 72(8):563–573, 2019.

[27] P.J. Stephens, F.J. Devlin, C.F. Chabalowski, and M.J. Frisch. Ab initio calculation of vibrational absorption and circular dichroism spectra using density functional force fields. *The Journal of Physical Chemistry*, 98(45):11623–11627, November 1994.

[28] A.D. Becke. Density-functional thermochemistry. III. the role of exact exchange. *The Journal of Chemical Physics*, 98(7):5648–5652, April 1993.

[29] C.J. Cramer and D.G. Truhlar. Density functional theory for transition metals and transition metal chemistry. *Physical Chemistry Chemical Physics*, 11(46):10757–10816, 2009.

[30] S. Grimme, J. Antony, S. Ehrlich, and H. Krieg. A consistent and accurate ab initio parametrization of density functional dispersion correction (dft-d) for the 94 elements h-pu. *The Journal of chemical physics*, 132(15):154104, 2010.

[31] L. Goerigk and S. Grimme. A thorough benchmark of density functional methods for general main group thermochemistry, kinetics, and noncovalent interactions. *Physical Chemistry Chemical Physics*, 13(14):6670–6688, 2011.

[32] J. G.t Brandenburg, C. Bannwarth, A. Hansen, and S. Grimme. B97-3c: A revised low-cost variant of the b97-d density functional method. *The Journal of chemical physics*, 148(6):064104, 2018.

[33] E. Caldeweyher and J.G. Brandenburg. Simplified dft methods for consistent structures and energies of large systems. *Journal of Physics: Condensed Matter*, 30(21):213001, 2018.

[34] C. van Wüllen. A relativistic kohn–sham density functional procedure by means of direct perturbation theory. *The Journal of chemical physics*, 103(9):3589–3599, 1995.

[35] P. Pyykko. Relativistic effects in structural chemistry. *Chemical Reviews*, 88(3):563–594, 1988.

[36] T. Saue. Relativistic hamiltonians for chemistry: A primer. *ChemPhysChem*, 12(17):3077–3094, 2011.

[37] W. Liu. Ideas of relativistic quantum chemistry. *Molecular Physics*, 108(13):1679–1706, 2010.

[38] K.G. Dyall and K. Fægri Jr. *Introduction to relativistic quantum chemistry*. Oxford University Press, 2007.

[39] P. Tecmer, K. Boguslawski, and D. Kedziera. Relativistic methods in computational quantum chemistry. *Handbook of computational chemistry*, 2:885–926, 2017.

[40] M. Barysz. Two-component relativistic theories. *Relativistic methods for chemists*, pages 165–190, 2010.

[41] C. Chang, M. Pelissier, and P.H. Durand. Regular two-component pauli-like effective hamiltonians in dirac theory. *Physica Scripta*, 34(5):394, 1986.

[42] E. van Lenthe, E. Baerends, and J.G. Snijders. Relativistic total energy using regular approximations. *The Journal of chemical physics*, 101(11):9783–9792, 1994.

[43] M. Dolg. Relativistic effective core potentials. In *Theoretical and computational chemistry*, volume 11, pages 793–862. Elsevier, 2002.

[44] N.B. Amor, S. Evangelisti, T. Leininger, and D. Andrae. Local orbitals in quantum chemistry. *Basis Sets in Computational Chemistry*, page 41, 2021.

[45] S. Lehtola and H. Jónsson. Pipek–mezey orbital localization using various partial charge estimates. *Journal of chemical theory and computation*, 10(2):642–649, 2014.

[46] J.M. Foster and S.F. Boys. Canonical configurational interaction procedure. *Reviews of Modern Physics*, 32(2):300, 1960.

[47] S. F. Boys. Construction of some molecular orbitals to be approximately invariant for changes from one molecule to another. *Reviews of Modern Physics*, 32(2):296, 1960.

[48] I. Høyvik, B. Jansik, and P. Jørgensen. Orbital localization using fourth central moment minimization. *The Journal of chemical physics*, 137(22):224114, 2012.

[49] C. Edmiston and K. Ruedenberg. Localized atomic and molecular orbitals. *Reviews of Modern Physics*, 35(3):457, 1963.

[50] I. Hø yvik, B. Jansik, and P. Jørgensen. Pipek-mezey localization of occupied and virtual orbitals. *Journal of computational chemistry*, 34(17):1456–1462, 2013.

[51] J. Pipek and P.G. Mezey. A fast intrinsic localization procedure applicable for abinitio and semiempirical linear combination of atomic orbital wave functions. *The Journal of Chemical Physics*, 90(9):4916–4926, 1989.

[52] R.S. Mulliken. Electronic population analysis on lcao–mo molecular wave functions. i. *The Journal of Chemical Physics*, 23(10):1833–1840, 1955.

[53] P. Hunt. Lecture notes on molecular orbitals and population analysis, February 2008.

[54] G. Knizia. Intrinsic atomic orbitals: An unbiased bridge between quantum theory and chemical concepts. *Journal of chemical theory and computation*, 9(11):4834–4843, 2013.

[55] Sergey I Bokarev and Oliver Kühn. Theoretical x-ray spectroscopy of transition metal compounds. *Wiley Interdisciplinary Reviews: Computational Molecular Science*, 10(1):e1433, 2020.

[56] P. Glatzel, R. Alonso-Mori, and D. Sokaras. Hard x-ray photon-in/photon-out spectroscopy: instrumentation, theory and applications. *X-Ray Absorption and X-Ray Emission Spectroscopy: Theory and Applications*, 1, 2016.

[57] M. Rovezzi and P. Glatzel. Hard x-ray emission spectroscopy: a powerful tool for the characterization of magnetic semiconductors. *Semiconductor Science and Technology*, 29(2):023002, 2014.

[58] J. Kern, R. Alonso-Mori, R. Tran, J. Hattne, R.J. Gildea, N. Echols, C. Glöckner, J. Hellmich, H. Laksmono, R.G. Sierra, et al. Simultaneous femtosecond x-ray spectroscopy and diffraction of photosystem ii at room temperature. *Science*, 340(6131):491–495, 2013.

[59] U. Bergmann and P. Glatzel. X-ray emission spectroscopy. *Photosynthesis research*, 102(2):255–266, 2009.

[60] M. Petric and M. Kavčič. Chemical speciation via x-ray emission spectroscopy in the tender x-ray range. *Journal of Analytical Atomic Spectrometry*, 31(2):450–457, 2016.

[61] W. Błachucki, J. Czapla-Masztafiak, J. Sá, and J. Szlachetko. A laboratory-based double x-ray spectrometer for simultaneous x-ray emission and x-ray absorption studies. *Journal of Analytical Atomic Spectrometry*, 34(7):1409–1415, 2019.

[62] M. Szlachetko, M. Berset, J.C. Dousse, J. Hoszowska, and J. Szlachetko. High-resolution laue-type dumond curved crystal spectrometer. *Review of scientific instruments*, 84(9):093104, 2013.

[63] L. Von Hamos. Röntgenspektroskopie und abbildung mittels gekrümmter kristallreflektoren. *Naturwissenschaften*, 20(38):705–706, 1932.

[64] T. Johansson. Über ein neuartiges, genau fokussierendes röntgenspektrometer. *Zeitschrift für Physik*, 82(7-8):507–528, 1933.

[65] H.H. Johann. Die erzeugung lichtstarker röntgenspektren mit hilfe von konkavkristallen. *Zeitschrift für Physik*, 69(3):185–206, 1931.

[66] G.T. Seidler, D.R. Mortensen, A.J. Remesnik, J.I. Pacold, N.A. Ball, N. Barry, M. Styczinski, and O.R. Hoidn. A laboratory-based hard x-ray monochromator for high-resolution x-ray emission spectroscopy and x-ray absorption near edge structure measurements. *Review of scientific instruments*, 85(11):113906, 2014.

[67] F. Neese. The orca program system. *Wiley Interdisciplinary Reviews: Computational Molecular Science*, 2(1):73–78, 2012.

[68] F. Neese. Software update: the orca program system, version 4.0. *Wiley Interdisciplinary Reviews: Computational Molecular Science*, 8(1):e1327, 2018.

[69] A.D. Becke. Density-functional thermochemistry. v. systematic optimization of exchange-correlation functionals. *The Journal of chemical physics*, 107(20):8554–8560, 1997.

[70] F. Weigend and R. Ahlrichs. Balanced basis sets of split valence, triple zeta valence and quadruple zeta valence quality for h to rn: Design and assessment of accuracy. *Physical Chemistry Chemical Physics*, 7(18):3297–3305, 2005.

[71] D. Andrae, U. Haeussermann, M. Dolg, H. Stoll, and H. Preuss. Energy-adjusted ab initio pseudopotentials for the second and third row transition elements. *Theoretica chimica acta*, 77(2):123–141, 1990.

[72] R. Sure and S. Grimme. Corrected small basis set hartree-fock method for large systems. *Journal of computational chemistry*, 34(19):1672–1685, 2013.

[73] S. Grimme. Semiempirical gga-type density functional constructed with a long-range dispersion correction. *Journal of computational chemistry*, 27(15):1787–1799, 2006.

[74] G. Knizia and J.E.M.N. Klein. Electron flow in reaction mechanisms—revealed from first principles. *Angewandte Chemie International Edition*, 54(18):5518–5522, 2015.

[75] J.C. Kromann. Calculate root-mean-square deviation (rmsd) of two molecules using rotation, 2021. `https://github.com/charnley/rmsd`.

[76] W. Kabsch. A solution for the best rotation to relate two sets of vectors. *Acta Crystallographica Section A: Crystal Physics, Diffraction, Theoretical and General Crystallography*, 32(5):922–923, 1976.

[77] EasyXAFS. easyxes100. `http://easyxafs.com/products/`.

[78] W.T. Elam, B.D. Ravel, and J.R. Sieber. A new atomic database for x-ray spectroscopic calculations. *Radiation Physics and Chemistry*, 63(2):121–128, 2002.

[79] B. Ravel and M. Newville. Athena, artemis, hephaestus: data analysis for x-ray absorption spectroscopy using ifeffit. *Journal of synchrotron radiation*, 12(4):537–541, 2005.

[80] S. Lafuerza, A. Carlantuono, M. Retegan, and P. Glatzel. Chemical sensitivity of kβ and kα x-ray emission from a systematic investigation of iron compounds. *Inorganic Chemistry*, 59(17):12518–12535, 2020.

[81] C.F. Shaw III, M.P. Cancro, and I.S. Butler. A high yield synthesis of dimethylsulfide-d6, and preparation of chloro-(dimethylsulfide-d6) gold (i) and trichloro (dimethylsulfide-d6) gold (iii). *Journal of Labelled Compounds and Radiopharmaceuticals*, 16(6):827–831, 1979.

[82] I.S. Butler, A. Neppel, K.R. Plowman, and C.F. Shaw III. Vibrational spectra and normal coordinate calculations for some dimethyl sulfide complexes of gold (i) and gold (iii). *Journal of Raman spectroscopy*, 15(5):310–318, 1984.

[83] F. Neese. *ORCA manual 4.1.0*. Max-Planck-Institut fur Kohlenforschung, 2018.

A Localization procedure using ZORA on all geometries

Atom	Population coefficients			Atom	Population coefficients		
	B97-3c	B97-D3	ZORA[a]		B97-3c	B97-D3	ZORA[a]
Complex 1							
Au	0.282	0.281	0.281	N	0.728	0.728	0.728
Au	0.282	0.281	0.281	N	0.728	0.728	0.728
Au	0.255	0.253	0.254	N	0.736	0.737	0.738
Au	0.357	0.358	0.356	Cl	0.631	0.630	0.632
Complex 3							
Au	0.232	0.230	0.230	N	0.757	0.759	0.760
Au	0.371	0.372	0.371	C	0.658	0.658	0.660
Au	0.371	0.372	0.370	C	0.658	0.658	0.660
Au	0.259	0.261	0.261	Cl	0.717	0.715	0.716
Complex 6							
Au	0.224	0.228	0.225	C	0.819	0.816	0.818
Au	0.183	0.185	0.184	Cl	0.801	0.799	0.800
Complex 7							
Au	0.226	0.223	0.223	P	0.789	0.791	0.792
Au	0.190	0.191	0.190	Cl	0.794	0.793	0.794
Complex 8							
Au	0.199	0.199	0.200	S	0.794	0.794	0.793
Au	0.233	0.232	0.231	Cl	0.762	0.763	0.764
Complex 9 [b]							
Au	0.296	0.297	0.296	Br	0.676	0.675	0.675
Complex 5 [b]							
Au	0.276	0.276	0.275	Cl	0.701	0.701	0.702
Complex 10 [b]							
Au	0.224	0.223	0.222	F	0.764	0.764	0.765
Complex 11							
Au	0.484	0.483	0.482	Cl	0.510	0.511	0.512
Au	0.282	0.282	0.283	Cl	0.682	0.682	0.681
Au	0.281	0.281	0.279	Cl	0.682	0.682	0.685

Table A.1: Population coefficients of localized orbitals for complexes performing the localization procedure at the B97-D3 ZORA level, on the optimized geometries obtained using the different methods. Any values that stand out are marked in red. [a] *B97-D3 ZORA is abbreviated as ZORA.* [b] *For these complexes all bond-like orbitals have the same coefficients due to the high symmetry.*

Compound	Mode	Crystal	Detector Angle (°)	Source angle (°)	Offset (°)	Transition	Zone 1	Zone 2	Zone 3	Number of Scans
Au Foil	XES	Si933	77.9775	78.026	-0.0485	Lβ_5	11550-11690 eV ΔE =0.5 eV, Δt=2.0 s	11690-11850 eV ΔE =2.0 eV, Δt=0.5 s	11850-11960 eV ΔE =0.5 eV, Δt=2.0 s	5
$HAuBr_4$	XES	Si933	77.9775	78.026	-0.0485	Lβ_5	11550-11690 eV ΔE =0.5 eV, Δt=2.0 s	11690-11850 eV ΔE =2.0 eV, Δt=0.5 s	11850-11960 eV ΔE =0.5 eV, Δt=2.0 s	5
Ph_3PAuCl	XES	Si933	77.9775	78.026	-0.0485	Lβ_5	11550-11690 eV ΔE =0.5 eV, Δt=2.0 s	11690-11850 eV ΔE =2.0 eV, Δt=0.5 s	11850-11960 eV ΔE =0.5 eV, Δt=2.0 s	5
$AuCl_3$	XES	Si933	77.9775	78.026	-0.0485	Lβ_5	11550-11620 eV ΔE =0.5 eV, Δt=2.0 s	11620-11850 eV ΔE =2.0 eV, Δt=0.5 s	11850-11960 eV ΔE =0.5 eV, Δt=2.0 s	7
DMSAuCl	XES	Si933	77.9775	78.026	-0.0485	Lβ_5	11550-11620 eV ΔE =0.5 eV, Δt=2.0 s	11620-11850 eV ΔE =2.0 eV, Δt=0.5 s	11850-11960 eV ΔE =0.5 eV, Δt=2.0 s	5
CNCAuCl	XES	Si933	77.9775	78.026	-0.0485	Lβ_5	11550-11620 eV ΔE =0.5 eV, Δt=2.0 s	11620-11850 eV ΔE =2.0 eV, Δt=0.5 s	11850-11960 eV ΔE =0.5 eV, Δt=2.0 s	5

Table B.1: Details on the XES measurements per sample

B Experimental Details XES

C NMR spectra

C.1 Complex 3

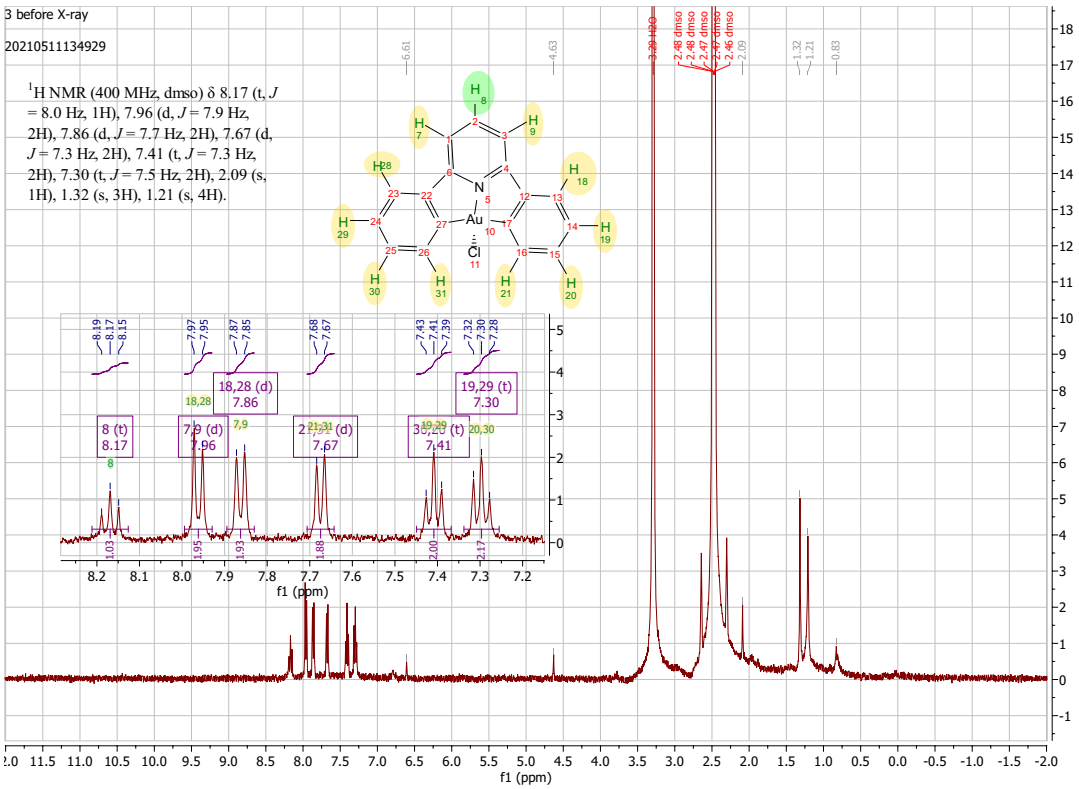

Figure C.1: ^{1}H-NMR-spectrum of complex 3 before XES

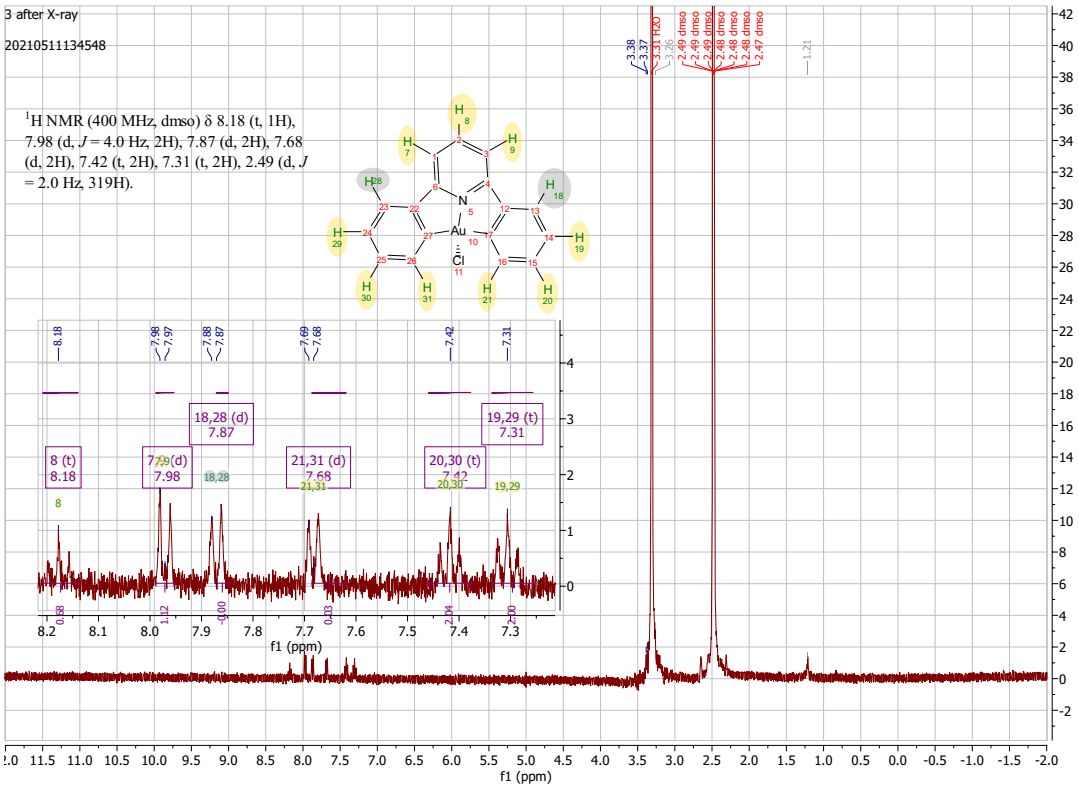

Figure C.2: ^{1}H-NMR-spectrum of complex 3 after XES

C.2 Complex 7

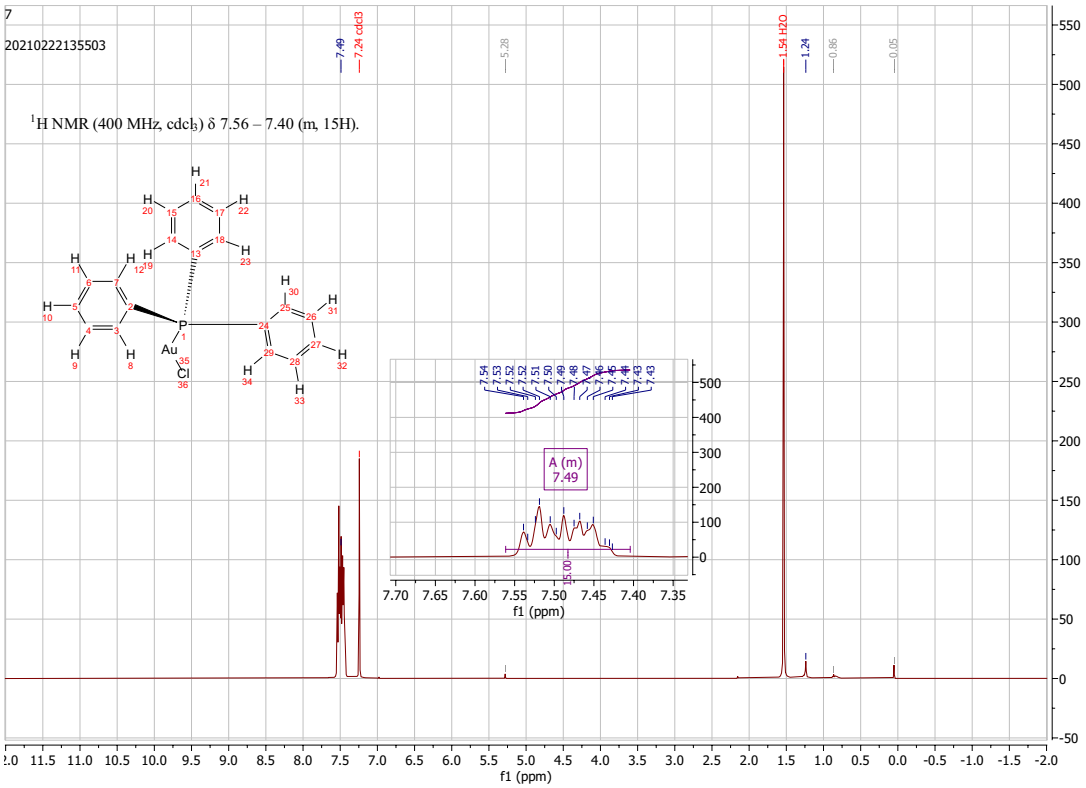

Figure C.3: ^{1}H-NMR-spectrum of complex 7 as provided by the Klein group

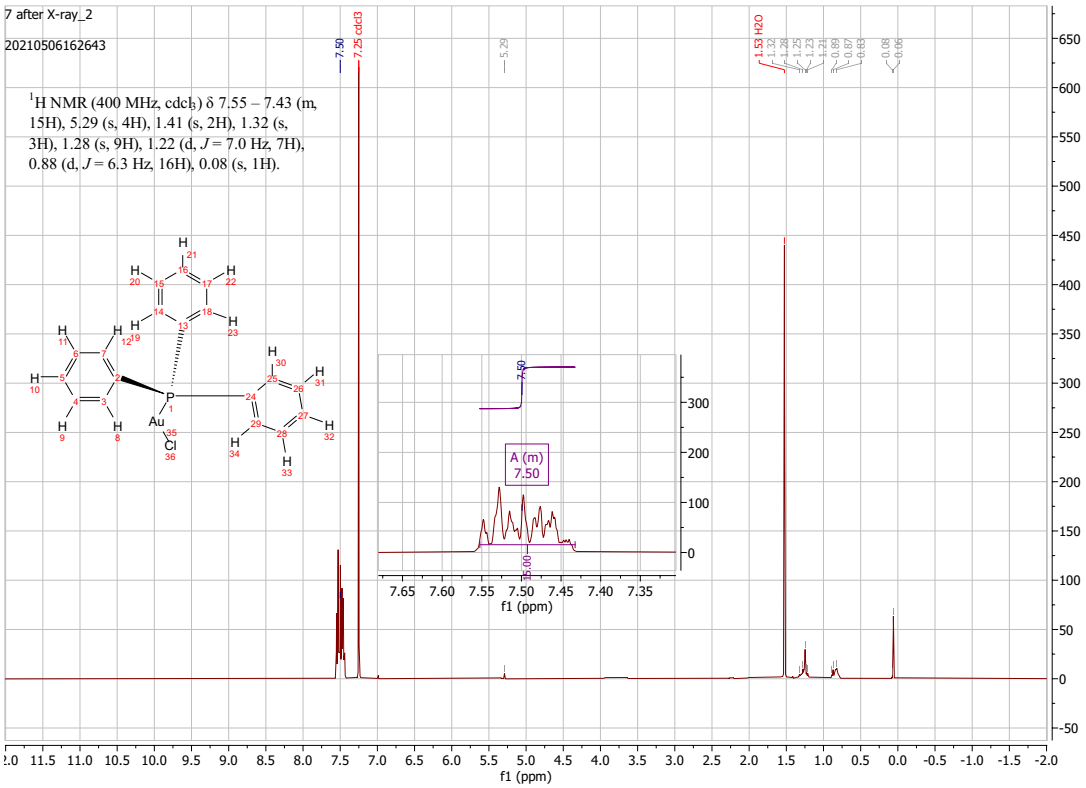

Figure C.4: ^{1}H-NMR-spectrum of complex 7 after XES

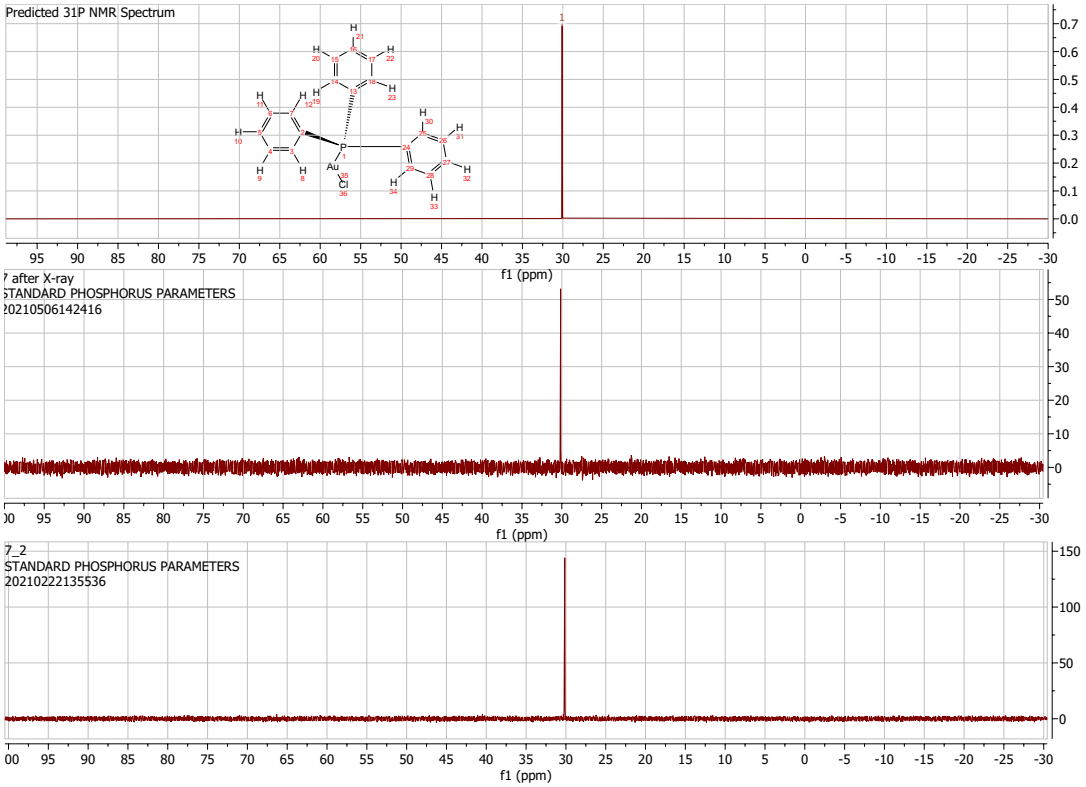

Figure C.5: ^{31}P-NMR-spectrum of complex

C.3 Complex 8

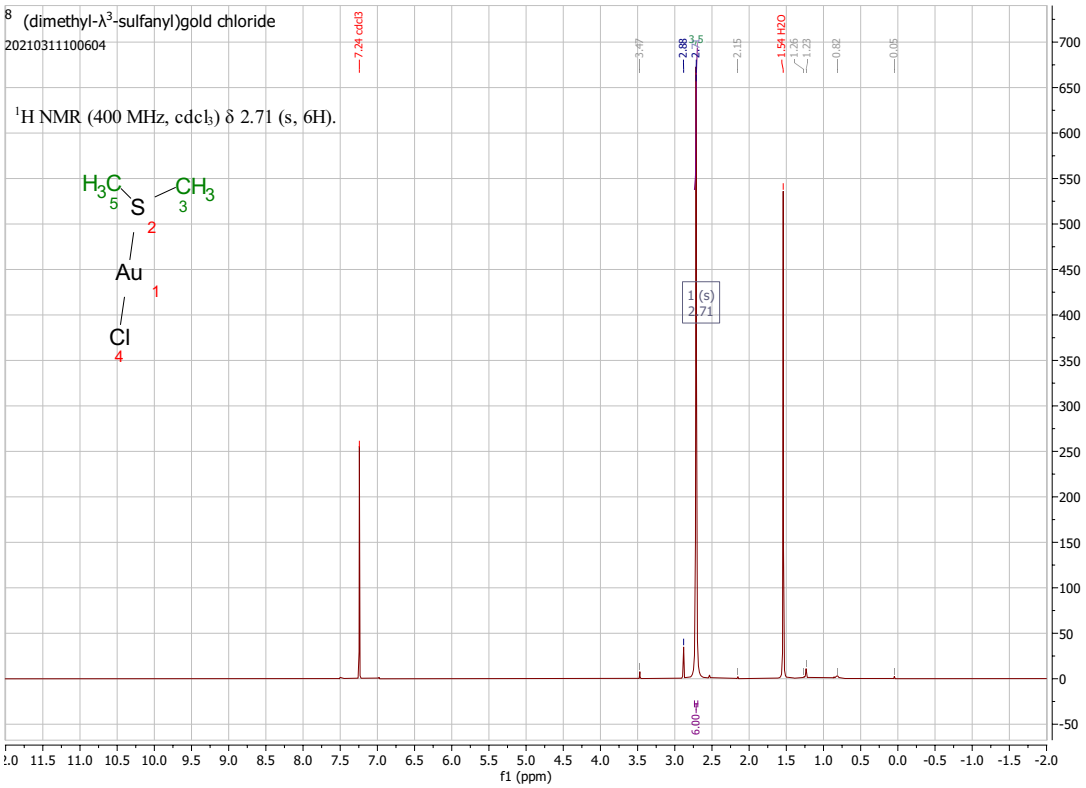

Figure C.6: [1]H-NMR-spectrum of complex 8 as provided by the Klein group

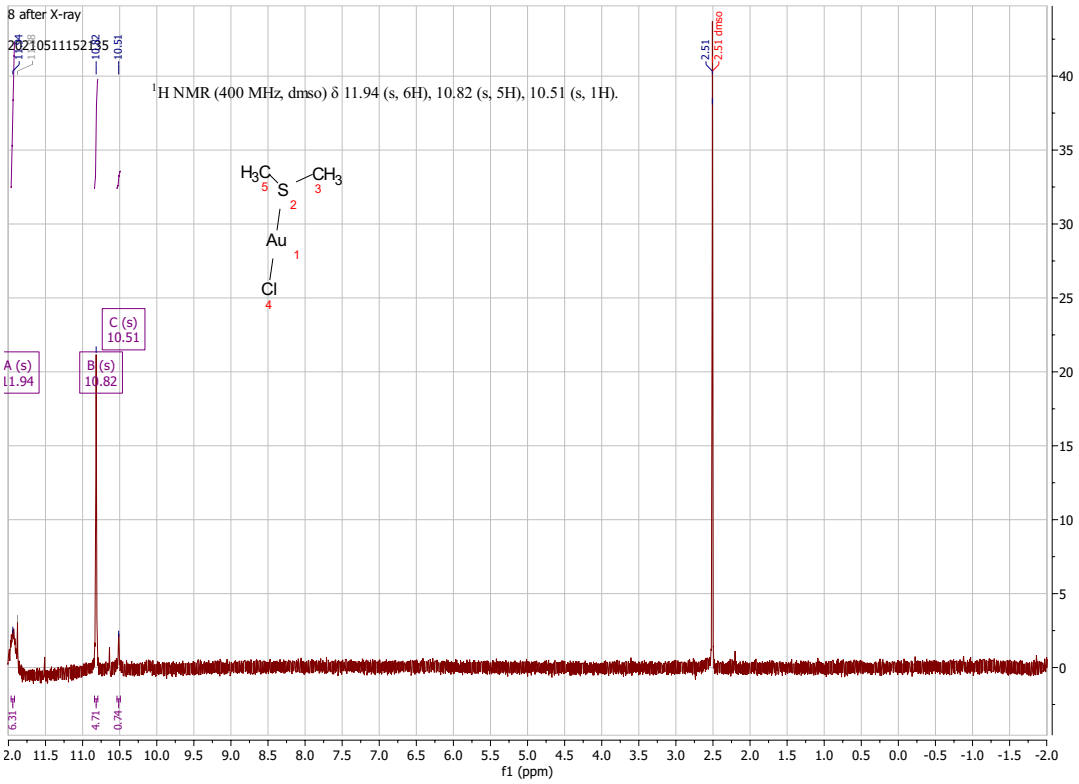

Figure C.7: ^{1}H-NMR-spectrum of complex 8 after XES

D Optimized geometries

Name: complex 1	**Method:** B97-3c
Optimized geometry (xyz) format	**Energies (Hartree)**
31 Coordinates from ORCA-job orca C 0.00000032779489 1.21252157120134 -3.36657872005093 C 0.00000070529821 0.00000000657977 -4.04654417053874 C 0.00000049681601 -1.21252156346797 -3.36657871568638 C 0.00000235885877 -1.20008978959063 -1.97848686914237 N 0.00000653103783 0.00000002449843 -1.36901370196052 C 0.00000224782654 1.20008982208499 -1.97848688515778 H -0.00000209389496 2.14209684914488 -3.91451000387792 H -0.00000027396847 -0.00000005569033 -5.12668634933638 H -0.00000178909310 -2.14209684600256 -3.91451002713222 Au -0.00000442468855 0.00000006440560 0.61848612697953 Cl 0.00000528433748 0.00000025798476 2.89878640894261 C -0.00000166301943 -2.33774088416505 -1.05500995156073 C 0.00000042485985 -3.66543543877272 -1.43727263619460 C 0.00000077349707 -4.66510816797014 -0.47124782665683 C 0.00000066338901 -4.32014287022714 0.86813856772880 C -0.00000234813850 -2.97986410354073 1.22154354841290 N -0.00000443064629 -2.02850143112008 0.28483064341807 H 0.00000204114646 -3.92591645255508 -2.48492731075760 H 0.00000174623755 -5.70309797636866 -0.77062083084856 H 0.00000234566204 -5.06809322770344 1.64673436901764 H -0.00000437955160 -2.64894579326555 2.24835124424613 C -0.00000178016255 2.33774089993273 -1.05500994456417 C 0.00000022234780 3.66543542647156 -1.43727262632219 C 0.00000077451085 4.66510813298024 -0.47124779769443 C 0.00000081842992 4.32014282880878 0.86813857804113 C -0.00000213853470 2.97986407704845 1.22154356034240 N -0.00000439554256 2.02850143818116 0.28483064125724 H 0.00000168948515 3.92591640389753 -2.48492730039445 H 0.00000170179345 5.70309793659588 -0.77062078613062 H 0.00000263996091 5.06809315788332 1.64673439890768 H -0.00000407604906 2.64894570274067 2.24835122437615	E = -1337.61341572 $E_{B97\text{-}D3/def2\text{-}TZVP\ ZORA}$ = -20884.206614315106

Name: complex 1	**Method:** B97-D3/def2-TZVP
Optimized geometry (xyz) format	**Energies (Hartree)**
31 Coordinates from ORCA-job orca C 0.00048734555152 1.21913903138818 -3.38007681240128 C 0.00076775473109 0.00000003984377 -4.06478911912705 C 0.00048740258200 -1.21913901711321 -3.38007690970396 C -0.00011993301984 -1.20483728124678 -1.98402704154863 N -0.00045628938332 -0.00000005412153 -1.37232499095192 C -0.00011993123853 1.20483719824684 -1.98402697345606 H 0.00077453620184 2.15526204987599 -3.92686845770442 H 0.00124098617786 0.00000008214528 -5.15068568870781 H 0.00077465580567 -2.15526199049678 -3.92686868603849 Au -0.00076791080003 0.00000001327066 0.62030751112402 Cl 0.00936812900188 -0.00000002430173 2.89637104707767 C -0.00039001100391 -2.34737501850370 -1.05445230442980 C -0.00035911180065 -3.68231481249338 -1.43952312078486 C -0.00057517634761 -4.68739840708500 -0.46791092673465 C -0.00080655205160 -4.33854472517252 0.87877810244673 C -0.00081242075824 -2.98975783042735 1.23208058642658 N -0.00062372682828 -2.03525645597565 0.29063829985480 H -0.00015588768750 -3.94026088539419 -2.49309008254016 H -0.00054273122343 -5.73099821452063 -0.76798842681301 H -0.00100150219522 -5.08865022851509 1.66282491566365 H -0.00095132421066 -2.65423194576415 2.26363450121308 C -0.00039005575751 2.34737496615418 -1.05445228919085 C -0.00035920392909 3.68231475725775 -1.43952315388553 C -0.00057520613488 4.68739834467469 -0.46791095547855 C -0.00080646763779 4.33854473691303 0.87877808459862 C -0.00081231700702 2.98975786693824 1.23208061361114 N -0.00062369027729 2.03525648009598 0.29063833806957 H -0.00015606563999 3.94026087515986 -2.49309012435343	E = -1337.86023259 $E_{B97\text{-}D3/def2\text{-}TZVP\ ZORA}$ = -20884.207607327455

H -0.00054279830072 5.73099814071641 -0.76798848853196 H -0.00100134766717 5.08865027389271 1.66282486174438 H -0.00095114915156 2.65423203455811 2.26363454821507	

Name: complex 1	**Method:** B97-D3/def2-TZVP ZORA
Optimized geometry (xyz) format	**Energies (Hartree)**
31 Coordinates from ORCA-job orca C 0.00007177043765 1.21889645383528 -3.38130702121463 C 0.00016951217227 0.00000009733217 -4.06602330252943 C 0.00007187471117 -1.21889633814416 -3.38130712660013 C -0.00019934593052 -1.20447816626529 -1.98565969744211 N -0.00044613942425 -0.00000003398965 -1.37307347367139 C -0.00019942254243 1.20447813048214 -1.98565963399887 H 0.00027140125694 2.15505026874701 -3.92797089015788 H 0.00038991191490 0.00000015505203 -5.15190502617610 H 0.00027155778892 -2.15505009526898 -3.92797113685480 Au 0.00027876443489 0.00000002951617 0.61364749629602 Cl 0.00129044419755 -0.00000001222470 2.88149957224900 C -0.00012735992621 -2.34564239960749 -1.05541052240134 C -0.00037967890676 -3.68092378307145 -1.43792849449664 C -0.00032478394873 -4.68377079599743 -0.46430059993238 C -0.00001794342311 -4.33189833276261 0.88139698189844 C 0.00025630813817 -2.98284643256766 1.23200239639944 N 0.00020414269897 -2.02979582343119 0.28875165796670 H -0.00063551420498 -3.94099888159703 -2.49093043094963 H -0.00051972600879 -5.72802058836860 -0.76203981390824 H -0.00001619370609 -5.08031098260476 1.66703321634980 H 0.00057554785263 -2.64529304417591 2.26274941982329 C -0.00012739648253 2.34564234611744 -1.05541050912552 C -0.00037971573732 3.68092369995666 -1.43792856153804 C -0.00032476835884 4.68377072367448 -0.46430068461459 C -0.00001791152939 4.33189830458812 0.88139691685502 C 0.00025631649080 2.98284643019824 1.23200238270191 N 0.00020412482258 2.02979580952167 0.28875167174179 H -0.00063555636704 3.94099877408695 -2.49093051787301 H -0.00051967376336 5.72802049773015 -0.76203992875548 H -0.00001612917816 5.08031096030359 1.66703312358042 H 0.00057558252109 2.64529302893484 2.26274939404130	E = -20890.91770710 $E_{B97\text{-}D3/def2\text{-}TZVP\ ZORA}$ = -20884.207750265312

Name: complex 3	**Method:** B97-3c
Optimized geometry (xyz) format	**Energies (Hartree)**
31 Coordinates from ORCA-job orca C -0.00002641545030 1.20723648554747 3.37282841068657 C -0.00003549172270 0.00000000662733 4.05359604855442 C -0.00002635482946 -1.20723643786298 3.37282837310626 C -0.00000605018994 -1.20305613078890 1.98133217542339 N 0.00001015578026 0.00000000999925 1.36187680815157 C -0.00000611371149 1.20305614615708 1.98133220201489 H -0.00003956133677 2.14177295464181 3.91146033730589 H -0.00005168892849 -0.00000004167938 5.13493602516516 H -0.00003935710414 -2.14177291353551 3.91146030370443 Au -0.00002817291179 0.00000004595070 -0.64101643864432 Cl -0.00008216410653 -0.00000013876193 -2.94359168262343 C -0.00000089939381 -2.34430612893605 1.07425720869374 C 0.00002489496361 -3.66930902652898 1.51339772647790 C 0.00003644649166 -4.70177596628952 0.59162337694791 C 0.00002187534791 -4.41935404948473 -0.76911661032049 C -0.00000580200881 -3.10147919740976 -1.21528825937959 C -0.00001553284046 -2.05533442822227 -0.31188980800949 H 0.00003505510932 -3.90339160410445 2.57037289074651 H 0.00005649732273 -5.72780739939876 0.93368007119586 H 0.00003378428198 -5.23073186222759 -1.48599481240861 H -0.00002081954861 -2.88639611620976 -2.27533391079301 C -0.00000096714236 2.34430612818969 1.07425725995072 C 0.00002471967622 3.66930905042482 1.51339779952143	E = -1304.88266470 $E_{B97\text{-}D3/def2\text{-}TZVP\ ZORA}$ = -20851.409913987973

C 0.00003646811884 4.70177596911249 0.59162340987382 C 0.00002193331012 4.41935406657144 -0.76911659280965 C -0.00000564984713 3.10147919017690 -1.21528825736688 C -0.00001546100136 2.05533437224641 -0.31188979788198 H 0.00003485286765 3.90339172270247 2.57037296085148 H 0.00005640083169 5.72780741482298 0.93368007925094 H 0.00003395388405 5.23073186368159 -1.48599481742130 H -0.00002053591191 2.88639601458816 -2.27533388841954	

Name: complex 3	**Method:** B97-D3/def2-TZVP
Optimized geometry (xyz) format	**Energies (Hartree)**
31 Coordinates from ORCA-job orca C -0.00020547928580 1.21365714432006 3.38275286962986 C -0.00035672031772 0.00000010517815 4.06816034769621 C -0.00020562553026 -1.21365698373551 3.38275290251794 C 0.00008564016535 -1.20779273501054 1.98339584620272 N 0.00017188304787 0.00000000772276 1.36109012852364 C 0.00008572978984 1.20779276774716 1.98339584385114 H -0.00028198341864 2.15423129003089 3.92069528406732 H -0.00057123235448 0.00000009402310 5.15490726066838 H -0.00028221406609 -2.15423107652649 3.92069534812466 Au 0.00102303090900 -0.00000002486011 -0.64950787664467 Cl -0.00905063822126 -0.00000012875013 -2.94734636100803 C 0.00034158654898 -2.35609325671071 1.07227723087865 C 0.00007358496934 -3.68696474666162 1.51818414371548 C 0.00023419488367 -4.72793008141172 0.59405414188909 C 0.00065260580212 -4.44675356532570 -0.77511315451498 C 0.00092948974195 -3.12240109235919 -1.22774278523126 C 0.00080271464302 -2.06749353921825 -0.32201425293286 H -0.00028911229527 -3.91581556766288 2.58118220370948 H 0.00001251449005 -5.75798490956419 0.93997370334546 H 0.00075794358529 -5.26383684517448 -1.49327539728838 H 0.00127834187368 -2.90991520271786 -2.29379268218021 C 0.00034167075699 2.35609323792352 1.07227723946440 C 0.00007364168109 3.68696467939785 1.51818416102162 C 0.00023414979602 4.72793005298050 0.59405423030945 C 0.00065257447792 4.44675355293301 -0.77511307548116 C 0.00092945024122 3.12240104912751 -1.22774269029119 C 0.00080276368721 2.06749346721586 -0.32201418186426 H -0.00028907310544 3.91581548704797 2.58118222281697 H 0.00001250159119 5.75798486502222 0.93997383202226 H 0.00075779930611 5.26383686017660 -1.49327531727857 H 0.00127826660705 2.90991509484222 -2.29379257419460	E = -1305.11332176 $E_{\text{B97-D3/def2-TZVP ZORA}}$ = -20851.410918996295

Name: complex 3	**Method:** B97-D3/def2-TZVP ZORA
Optimized geometry (xyz) format	**Energies (Hartree)**
31 Coordinates from ORCA-job orca C 0.00000647744311 1.21350354447554 3.38534098620646 C 0.00000514936827 0.00000004429498 4.07075936457230 C 0.00000647334664 -1.21350351024920 3.38534108793863 C -0.00001005805507 -1.20748169551547 1.98631711180694 N -0.00006604767799 -0.00000005030274 1.36333518014159 C -0.00001005245456 1.20748162181009 1.98631701917728 H 0.00002982305940 2.15412151248271 3.92324473466746 H 0.00001261866625 0.00000007406040 5.15753889849498 H 0.00002983692816 -2.15412142001356 3.92324497967739 Au 0.00006391024897 0.00000002407948 -0.64048852779961 Cl 0.00009325876875 0.00000004172489 -2.93035695464483 C 0.00001986101584 -2.35393898427678 1.07374733160817 C -0.00002970371372 -3.68551353540270 1.51613062151174 C -0.00004541416191 -4.72348979002862 0.58884609337743 C -0.00002601716400 -4.43796462611273 -0.77923921714939 C 0.00003733773683 -3.11256072257655 -1.22793566639831 C 0.00006814045476 -2.05991060005536 -0.31933364122239 H -0.00004992514144 -3.91769488416719 2.57844792964204	E = -20858.12347146 $E_{\text{B97-D3/def2-TZVP ZORA}}$ = -20851.411095796822

H -0.00007047286649 -5.75466194094267 0.93153025536966 H -0.00005580016563 -5.25293535745836 -1.49986219175164 H 0.00007129795457 -2.89721963224481 -2.29339901321288 C 0.00001992354566 2.35393890762822 1.07374721722189 C -0.00002977232684 3.68551339800626 1.51613057483146 C -0.00004535359393 4.72348970052680 0.58884612909445 C -0.00002604189153 4.43796467061710 -0.77923920904850 C 0.00003732314033 3.11256081266732 -1.22793576198056 C 0.00006813089955 2.05991064116058 -0.31933377098047 H -0.00004995099862 3.91769469983012 2.57844789466658 H -0.00007048475214 5.75466181020518 0.93153038081501 H -0.00005578169849 5.25293545013477 -1.49986211932473 H 0.00007131408524 2.89721979564233 -2.29339912576356	

Name: complex 6	**Method:** B97-3c
Optimized geometry (xyz) format	**Energies (Hartree)**
67 Coordinates from ORCA-job orca Au -0.00009708010491 -0.00000126480554 1.26065673321387 C 0.00004200409087 -0.00000034887855 -0.70709158376884 N 0.00007200012852 1.07115445697588 -1.53924579666622 C 0.00013119175252 0.67614412459067 -2.86476051547657 C 0.00013094388604 -0.67614355925472 -2.86476098602999 N 0.00007287840981 -1.07115469933478 -1.53924646555231 H 0.00015679223402 -1.38912930100454 -3.66719664525787 H 0.00015709031658 1.38913031202646 -3.66719579566149 C 0.00001843917793 -2.43012396476562 -1.08194730071390 C 1.22892614058054 -3.05424372900138 -0.85609477214224 C 1.20067323559165 -4.37183903315669 -0.41074938465972 C -0.00010657741525 -5.02517037063022 -0.19464749593412 C -1.20082318824455 -4.37172218286114 -0.41074599702454 C -1.22894721207717 -3.05412701252073 -0.85609886632888 H 2.13058976354813 -4.88802045771700 -0.21645587576887 H -0.00015592998753 -6.04812171497734 0.15738736542012 H -2.13078976587303 -4.88781115334558 -0.21644649076635 C 0.00001668249089 2.43012339433588 -1.08194584027472 C 1.22892401128170 3.05424254743674 -0.85609060822590 C 1.20067079133637 4.37183794603053 -0.41074552177026 C -0.00010915695682 5.02517025229093 -0.19464735614494 C -1.20082554137839 4.37172227259508 -0.41074769541685 C -1.22894917605158 3.05412704091020 -0.85610043243318 H 2.13058713911997 4.88801897609871 -0.21645009085965 H -0.00015881117653 6.04812158826830 0.15738754589462 H -2.13079233519952 4.88781205050025 -0.21645135369646 C -2.54418972063619 2.33122766053871 -1.02811901525822 C -3.47179989121918 3.05386292278450 -2.00074688239838 H -2.33711541131948 1.34962650802413 -1.45130434821466 C -3.21185561933137 2.10227486468690 0.32669786445433 H -3.77235370262814 4.02980748891461 -1.62241240198225 H -2.99343448674890 3.20695858645751 -2.96751201522403 H -4.37939809919044 2.47268718103389 -2.16025686433235 H -2.55151730617391 1.56216016878296 1.00237069253584 H -3.47596511419714 3.04598063827256 0.80227047874293 H -4.12630149461019 1.52179448235404 0.20712801636712 C 2.54424026356120 2.33148196220163 -1.02811785145568 C 3.47175312895437 3.05419970165935 -2.00077688124521 C 3.21195897543670 2.10263531460024 0.32669082379226 H 2.33726756609974 1.34984973452169 -1.45127973400070 H 2.99335354737453 3.20722278976600 -2.96753659490750 H 3.77220629336377 4.03018506229925 -1.62246764618138 H 4.37941254012406 2.47312076813200 -2.16029111600776 H 3.47597224752307 3.04638197623158 0.80223591015324 H 2.55169577888832 1.56246240316981 1.00239005026117 H 4.12646754815046 1.52225519432796 0.20711577624967 C -2.54418751920408 -2.33122609472824 -1.02811312024629 C -3.47180263257564 -3.05386137669682 -2.00073624782574 C -3.21184736319781 -2.10227052652062 0.32670630151360	E = -1755.807498631268 $E_{B97\text{-}D3/def2\text{-}TZVP\ ZORA}$ = -21302.561755363557

H -2.33711347790595 -1.34962580241582 -1.45130062609957 H -2.99344124921689 -3.20695931540244 -2.96750300579306 H -3.77235641007982 -4.02980491940167 -1.62239909452355 H -4.37940059371946 -2.47268450007265 -2.16024365013513 H -3.47595585609452 -3.04597533949040 0.80228138819163 H -2.55150547910671 -1.56215571012889 1.00237553470554 H -4.12629306730920 -1.52178920739000 0.20713959859276 C 2.54424240532220 -2.33148379781766 -1.02812555783688 C 3.47175270763870 -3.05420266147071 -2.00078621784739 H 2.33726908585796 -1.34985181621514 -1.45128769329743 C 3.21196435507958 -2.10263657356406 0.32668143402094 H 3.77220660595969 -4.03018774328787 -1.62247680650811 H 2.99335067202654 -3.20722662471284 -2.96754457269072 H 4.37941182562356 -2.47312404303239 -2.16030333523468 H 2.55170295468619 -1.56246293871654 1.00238182963416 H 3.47597819272697 -3.04638309716288 0.80222652228731 H 4.12647292717226 -1.52225693190634 0.20710399811377 Cl -0.00025945658506 -0.00000255843112 3.56080092343614	

Name: complex 6	**Method:** B97-D3/def2-TZVP
Optimized geometry (xyz) format	**Energies (Hartree)**
67 Coordinates from ORCA-job orca Au 0.00031226107526 -0.00000174757568 1.28444921782863 C -0.00005573032699 -0.00000033622662 -0.69794959591741 N -0.00015022352291 1.07570428752361 -1.53552507686070 C -0.00029929909012 0.68005432229460 -2.86689516297605 C -0.00029882921118 -0.68005390726376 -2.86689547871852 N -0.00015211919132 -1.07570448783195 -1.53552562813933 H -0.00037196028239 -1.39788073192319 -3.67131038087429 H -0.00037259602037 1.39788148900801 -3.67130975792768 C -0.00003988521302 -2.44062303331486 -1.07990138540013 C 1.23604575256403 -3.06668480621503 -0.85335798851057 C 1.20814829285151 -4.39076921081554 -0.40311613061056 C 0.00021938155453 -5.04754597087438 -0.18468105880971 C -1.20784082193172 -4.39101196583969 -0.40312226985610 C -1.23600611769858 -3.06692545958333 -0.85334369073758 H 2.14335247329986 -4.90756252828036 -0.20850247263239 H 0.00032174535492 -6.07461950990792 0.17120039185625 H -2.14294135270905 -4.90799824519306 -0.20852305205623 C -0.00003607468702 2.44062268419575 -1.07990034984106 C 1.23605029110275 3.06668588986401 -0.85336410823642 C 1.20815386018295 4.39077027358284 -0.40312206155427 C 0.00022545085113 5.04754534558851 -0.18467910328368 C -1.20783528625800 4.39101005673060 -0.40311354078354 C -1.23600162683412 3.06692366763486 -0.85333523606032 H 2.14335859098464 4.90756482235787 -0.20851426332544 H 0.00032870083604 6.07461889799049 0.17120232668908 H -2.14293527238649 4.90799489514004 -0.20850778201898 C -2.55713287524464 2.33792344019560 -1.03070902616392 C -3.48774295314313 3.06689161993810 -2.01236138274715 H -2.34510047785935 1.35203212979258 -1.45570978775929 C -3.23605128610319 2.10804212709571 0.33051786025900 H -3.78061136731052 4.05100834369019 -1.63080782161309 H -3.00284238401525 3.21367803514375 -2.98387777226328 H -4.40309522555879 2.48511330925874 -2.16847471072621 H -2.57399221924767 1.56263823079619 1.01031684348514 H -3.49864710745817 3.06058008543259 0.80391917026013 H -4.15649141283331 1.52716316537897 0.20228583611160 C 2.55702156609830 2.33739300960536 -1.03071062909564 C 3.48784933605946 3.06619234387161 -2.01228280443851 C 3.23581143654134 2.10727663809234 0.33054083315750 H 2.34477767491262 1.35157086883053 -1.45576898710393 H 3.00302958798835 3.21313984327330 -2.98381513335281 H 3.78092842439110 4.05022212778256 -1.63066687124704 H 4.40307354637769 2.48420841364013 -2.16838120319431 H 3.49860713927633 3.05972578313927 0.80400954088442 H 2.57358335747977 1.56199245489546 1.01027232657430 H 4.15612101569951 1.52618561160380 0.20232804330527	E = -1756.150503499927 $E_{\text{B97-D3/def2-TZVP ZORA}}$ = -21302.563833609489

C -2.55713740051487 -2.33792735133380 -1.03072629761806 C -3.48774074667344 -3.06689798507772 -2.01238314796133 C -3.23606437797494 -2.10804561475992 0.33049626895618 H -2.34510395679127 -1.35203625540466 -1.45572703576446 H -3.00283421551668 -3.21368534610969 -2.98389641084475 H -3.78061055496004 -4.05101441444322 -1.63082989719281 H -4.40309265178482 -2.48512079063263 -2.16850276326054 H -3.49866093437409 -3.06058355272721 0.80389721462287 H -2.57401056672722 -1.56263947958433 1.01029856440082 H -4.15650493489835 -1.52716873093764 0.20225800088555 C 2.55701680962456 -2.33738922864996 -1.03069453211437 C 3.48785461636665 -3.06618743353233 -2.01225800209762 H 2.34477407688811 -1.35156810229553 -1.45575588003776 C 3.23579456501465 -2.10726942860374 0.33056239373879 H 3.78093338017954 -4.05021582819613 -1.63063824954743 H 3.00304327824999 -3.21313768434980 -2.98379410868253 H 4.40307846710215 -2.48420113407186 -2.16834967752566 H 2.57355954561483 -1.56198563340909 1.01028743841691 H 3.49858811005975 -3.05971733845397 0.80403473877104 H 4.15610402971652 -1.52617667362509 0.20235663589842 Cl 0.00073808005424 -0.00000426632426 3.57890869914210	

Name: complex 6	**Method:** B97-D3/def2-TZVP ZORA
Optimized geometry (xyz) format	**Energies (Hartree)**
67 Coordinates from ORCA-job orca Au -0.00058099536400 -0.00000024111613 1.27041880563998 C 0.00012434656631 0.00000002967288 -0.70027217626945 N 0.00030290465403 1.07567187455756 -1.53858782408295 C 0.00058878504916 0.67990925061315 -2.86967698327905 C 0.00058870500898 -0.67990914760324 -2.86967698954654 N 0.00030462656155 -1.07567178659699 -1.53858783043375 H 0.00072834628870 -1.39776122061630 -3.67400041352714 H 0.00072831389675 1.39776134761539 -3.67400040159999 C 0.00007708120475 -2.44035085051864 -1.08299518701262 C 1.23568302954164 -3.06689389388415 -0.85646887788825 C 1.20752035016365 -4.39063825753195 -0.40598077885979 C -0.00044058775490 -5.04674807728735 -0.18734124439415 C -1.20813979824147 -4.39015674428491 -0.40597657105439 C -1.23576880061324 -3.06641492771565 -0.85650096670293 H 2.14252206086240 -4.90768433875487 -0.21116679081939 H -0.00064481360168 -6.07376786691145 0.16880509205988 H -2.14334828494059 -4.90682098698694 -0.21114196238477 C 0.00007368083614 2.44035094968976 -1.08299528014250 C 1.23567903698905 3.06689284235266 -0.85646286777310 C 1.20751544092919 4.39063708513822 -0.40597448924929 C -0.00044597987895 5.04674811785119 -0.18734129015307 C -1.20814476723202 4.39015823204040 -0.40598334442877 C -1.23577287606962 3.06641625191506 -0.85650735492805 H 2.14251668573373 4.90768203078272 -0.21115525329153 H -0.00065101557436 6.07376795183949 0.16880489436992 H -2.14335371102911 4.90682356619369 -0.21115385767590 C -2.55631710998454 2.33670192769068 -1.03252434746196 C -3.49282114797633 3.06968229553433 -2.00478178673107 H -2.34456803131763 1.35382690905627 -1.46444340277012 C -3.22762992559187 2.09764968423259 0.33044365459236 H -3.78669879213918 4.05038883222242 -1.61536683820126 H -3.01271337022695 3.22426279171659 -2.97742132103280 H -4.40738743404639 2.48662735411280 -2.16067708107045 H -2.56190620598967 1.54670572605101 1.00223012686571 H -3.48651570554216 3.04707712136227 0.81206534157732 H -4.14926305765413 1.51840963536948 0.20333127212192 C 2.55653927932598 2.33775940184554 -1.03254025802114 C 3.49260826259845 3.07108134648224 -2.00495779944365 C 3.22811369485556 2.09916395832476 0.33037860513215 H 2.34520467380831 1.35474830716068 -1.46434847175284 H 3.01233353662653 3.22534910501096 -2.97756464802674 H 3.78607261427535 4.05195948937224 -1.61566329544624 H 4.40742795192932 2.48843375325877 -2.16088813764298	E = -21309.459823098525 $E_{B97\text{-}D3/def2\text{-}TZVP\ ZORA}$ = -21302.564019614179

H 3.48660577868346 3.04876434797801 0.81187160799798 H 2.56272802002755 1.54797663689382 1.00229799405680 H 4.15000502163220 1.52034627531338 0.20322346629074 C -2.55631290038371 -2.33669854356845 -1.03250982745512 C -3.49282459329532 -3.06967804949614 -2.00476055945797 C -3.22761599540375 -2.09764395874871 0.33046253251181 H -2.34456494570964 -1.35382418361799 -1.46443098585376 H -3.01272349778682 -3.22425998710230 -2.97740317340642 H -3.78670115354676 -4.05038385523411 -1.61534296995364 H -4.40739100999045 -2.48662179878300 -2.16065022798499 H -3.48650007517722 -3.04707050963228 0.81208685144847 H -2.56188670029399 -1.54670050246278 1.00224390017028 H -4.14924901734907 -1.51840245759726 0.20335597072080 C 2.55654343483812 -2.33776264622743 -1.03255451418243 C 3.49260435167077 -3.07108547602747 -2.00497913787367 H 2.34520775670040 -1.35475076846459 -1.46436040146886 C 3.22812783058325 -2.09916990726522 0.33035990704426 H 3.78606975389896 -4.05196440170245 -1.61568738424485 H 3.01232253323696 -3.22535170951739 -2.97758272589099 H 4.40742394152424 -2.48843934602694 -2.16091548393172 H 2.56274791810416 -1.54798200917511 1.00228450610793 H 3.48662147557238 -3.04877129262715 0.81185011523226 H 4.15001935950175 -1.52035382277389 0.20319895501266 Cl -0.00139828397415 -0.00000086339177 3.55511455361031	

Name: complex 7	**Method:** B97-3c
Optimized geometry (xyz) format	**Energies (Hartree)**
36 Coordinates from ORCA-job orca P 0.00097476643395 -0.00018011283640 0.61971982198600 C 1.67064040051563 -0.00758073289012 1.34694678302554 C 2.66050255524482 0.75757230824844 0.73214323986338 C 3.93105790182388 0.81771983141293 1.28053039452769 C 4.22513454052616 0.10741729974068 2.43725556930999 C 3.24419970503953 -0.66198295772111 3.04604033174205 C 1.96784712295186 -0.72030690262743 2.50514989319567 H 2.43521313366773 1.29259731303094 -0.18115576817116 H 4.69613397657166 1.40954408268753 0.79695670845723 H 5.22042239851354 0.14840088951771 2.85923708385340 H 3.47238026609646 -1.22322100433979 3.94206829849492 H 1.20806116866905 -1.32587179200452 2.97887138163100 C -0.84130060910354 -1.44257451955471 1.34533030829958 C -0.67254463773573 -2.68291053663809 0.73177448494280 C -1.25784525608082 -3.81258963629415 1.27941866680827 C -2.02296271608044 -3.71098628803701 2.43409897298532 C -2.19977953374101 -2.47628133652951 3.04162018483077 C -1.61016612400025 -1.34248617223309 2.50140662531509 H -0.09413222295602 -2.75645263680870 -0.17991853740331 H -1.12705544059648 -4.77147664919683 0.79685264218933 H -2.48663350137655 -4.59293806188027 2.85542806669782 H -2.80219227735499 -2.39238412761868 3.93603760390901 H -1.75546371599509 -0.38115734328268 2.97373110918367 C -0.82793622075174 1.44945855654363 1.34646280848053 C -1.99006206164604 1.91930983260687 0.73652732540039 C -2.67718417762878 2.98936230591735 1.28560338164717 C -2.20438430423550 3.60385308117594 2.43794328293741 C -1.04307027204528 3.14390348945933 3.04173644548396 C -0.35461750585229 2.06787336641965 2.50023772830988 H -2.34501985646454 1.45292108059443 -0.17323353891055 H -3.57590180806422 3.35217713448034 0.80590042627451 H -2.73748457883446 4.44513034399542 2.86031741594871 H -0.66755979785320 3.62567648912371 3.93437905532715 H 0.55298289835185 1.71584516290059 2.96998254811436 Au 0.00280044091733 0.00080184234545 -1.61980262953191 Cl 0.00494534307354 0.00181640029216 -3.92141186806640	E = -1632.197224602011 $E_{B97\text{-}D3/def2\text{-}TZVP\ ZORA}$ = -21179.909118781823

Name: complex 7			**Method:** B97-D3/def2-TZVP
Optimized geometry (xyz) format			**Energies (Hartree)**
36			E =-1632.514822288642
Coordinates from ORCA-job orca			
P	0.00122054822498	0.00005464733434	0.59897759728093	
C	1.67012238708116	-0.00818619491538	1.33573718997515	$E_{B97\text{-}D3/def2\text{-}TZVP\ ZORA}$ = -21179.910249712193
C	2.66822215972139	0.76900220059712	0.73026286860462	
C	3.94266494405515	0.82902930561774	1.28923395838871	
C	4.23387197454079	0.10631934508130	2.44865511046252	
C	3.24644554820709	-0.67633769866097	3.04811640026845	
C	1.96609376892727	-0.73381099373246	2.49635069410258	
H	2.44396033758853	1.31562765168418	-0.18226139939695	
H	4.71164242664136	1.43148233442411	0.81337611092157	
H	5.23128227333010	0.14680770517179	2.87833197101639	
H	3.47172219153270	-1.24639644010061	3.94561626188973	
H	1.20073457222553	-1.34566270300714	2.96393150501045	
C	-0.84134504011070	-1.44148581633484	1.33379855335232	
C	-0.66476228220044	-2.69523337897069	0.73054650222001	
C	-1.25222282662235	-3.82822553062560	1.28866157698975	
C	-2.02829695300650	-3.71767175948554	2.44488807353341	
C	-2.21481883619133	-2.47048689965759	3.04212497017966	
C	-1.62233903651952	-1.33365018455348	2.49117713317713	
H	-0.07556769028660	-2.77570926525170	-0.17950837467257	
H	-1.11302785935929	-4.79600207206312	0.81458397238219	
H	-2.49355864415254	-4.60123157053547	2.87377720348447	
H	-2.82466902652765	-2.37950126390370	3.93712472473481	
H	-1.77130173789968	-0.36418011881907	2.95665519424820	
C	-0.82699136037097	1.44912718916989	1.33553688093542	
C	-2.00522825410623	1.91810731836069	0.73655790815081	
C	-2.69451097795432	2.99127349778097	1.29637530833672	
C	-2.20831322339829	3.61121899973486	2.44993197947511	
C	-1.03078246038033	3.15426561380491	3.04276425317196	
C	-0.34073364475973	2.07461370711215	2.49026120516839	
H	-2.37176365550843	1.44555206499729	-0.17128917273789	
H	-3.60557337720927	3.35058654352055	0.82565734857261	
H	-2.74232094981153	4.45435247019373	2.88009985109037	
H	-0.64526405889737	3.63925843008361	3.93572613444227	
H	0.57614209028915	1.72231153358422	2.95275834336507	
Au	0.00332356603444	0.00159330642128	-1.64446721717935	
Cl	0.00594310687342	0.00318802594262	-3.94588437385572	

Name: complex 7			**Method:** B97-D3/def2-TZVP ZORA
Optimized geometry (xyz) format			**Energies (Hartree)**
36			E = -21186.807728002688
Coordinates from ORCA-job orca			
P	0.00117920811251	-0.00000994173164	0.60108691370592	
C	1.66991434986450	-0.00621958526559	1.33793009824599	$E_{B97\text{-}D3/def2\text{-}TZVP\ ZORA}$ = -21179.910463795266
C	2.66897664849585	0.76291229152726	0.72463449594220	
C	3.94439131096357	0.82302243563354	1.28090800858805	
C	4.23523659892263	0.10834676377518	2.44507786104911	
C	3.24660147810013	-0.66664111338901	3.05195427740257	
C	1.96530998926957	-0.72436480468679	2.50293755397571	
H	2.44444393436593	1.30260665612268	-0.19195214364748	
H	4.71461271264003	1.41922483406762	0.79916987021496	
H	5.23351444150127	0.14890737121299	2.87277033406122	
H	3.47184305977129	-1.23078852780772	3.95322312464318	
H	1.19907089271137	-1.33090421534055	2.97594691831118	
C	-0.83955564823282	-1.44231215470020	1.33619415071919	
C	-0.67084633131689	-2.69285424587294	0.72493548553075	
C	-1.25869652629711	-3.82668287568801	1.28047327099053	
C	-2.02718102452029	-3.71979040393446	2.44178157298233	
C	-2.20605990074034	-2.47539748193915	3.04661644423662	
C	-1.61336602118221	-1.33766715012569	2.49828872802646	
H	-0.08786057714363	-2.76965057733375	-0.18943589669395	
H	-1.12585816852770	-4.79240169102087	0.80035742302530	
H	-2.49279702669983	-4.60409265372198	2.86879391852931	
H	-2.81045938399929	-2.38729996228679	3.94562671887435	
H	-1.75709759811072	-0.37008268188422	2.96929253510079	

C -0.82856022503145 1.44796514989422 1.33774588487095 C -1.99969862876138 1.92260258584977 0.73021394301530 C -2.68952135420086 2.99659013558020 1.28732501116691 C -2.21068242143148 3.61139365706651 2.44637938992711 C -1.03977237244117 3.14876385964145 3.04735959163383 C -0.34904620512136 2.06842539746556 2.49759225105460 H -2.35957882160244 1.45391485606744 -0.18229699688792 H -3.59531916548950 3.36074287926964 0.81015318164549 H -2.74516171242675 4.45525615975476 2.87456969548657 H -0.65979088663638 3.63016951950426 3.94465765054946 H 0.56327296163552 1.71215308980932 2.96602466744876 Au 0.00307513488312 0.00136627215355 -1.63058913541822 Cl 0.00546727867633 0.00279615233337 -3.92156055121786	

Name: complex 8	**Method:** B97-3c
Optimized geometry (xyz) format	**Energies (Hartree)**
11 Coordinates from ORCA-job orca Au -2.55038716933264 0.20709760663619 0.02464255430285 S -2.25936625826366 2.31298527281031 0.90250522667096 C -0.76655197649240 2.97308182887247 0.08805112137606 C -3.52982038662547 3.34891303171971 0.10245966372711 Cl -2.83885468618978 -1.88415782572247 -0.82464470409959 H 0.07197271853464 2.37957195965611 0.43498669886541 H -0.63100819857469 4.00861094060554 0.38655534221174 H -0.84783467150506 2.88885474162645 -0.98970060191045 H -4.49289966892718 3.00118622416377 0.45926487148578 H -3.48559345425322 3.24665112050713 -0.97589427251981 H -3.38026934837051 4.38283829912477 0.39981059988994	E = -1074.177703362762 $E_{B97\text{-}D3/def2\text{-}TZVP\ ZORA}$ = -20621.812461250920

Name: complex 8	**Method:** B97-D3/def2-TZVP
Optimized geometry (xyz) format	**Energies (Hartree)**
11 Coordinates from ORCA-job orca Au -2.54485967647700 0.20161909246379 0.00465456786426 S -2.24882428621519 2.29465294685688 0.88189853264330 C -0.76773582820691 2.97936004221426 0.07228409718576 C -3.52650241597085 3.34519043486421 0.12040668358403 Cl -2.85339202003690 -1.89464150732482 -0.82260464486106 H 0.08055835986083 2.37965875004012 0.40715947266728 H -0.64187239011486 4.01676514546775 0.39414557655844 H -0.86062332701608 2.91491871638028 -1.01310348970941 H -4.48935105078320 2.98720188453350 0.48950358333184 H -3.49315996804516 3.26282047695614 -0.96721234801487 H -3.36485049699465 4.37808721754786 0.44090446875044	E = -1074.403752701351 $E_{B97\text{-}D3/def2\text{-}TZVP\ ZORA}$ = -20621.812820772579

Name: complex 8	**Method:** B97-D3/def2-TZVP ZORA
Optimized geometry (xyz) format	**Energies (Hartree)**
11 Coordinates from ORCA-job orca Au -2.54429914150591 0.21004549894993 0.00660354110801 S -2.25033722069666 2.28933138979237 0.88079520021294 C -0.76965415645069 2.97550735642475 0.07138191378612 C -3.52635455247832 3.34334910081815 0.12016144146109 Cl -2.84647819485372 -1.87719431899463 -0.81900957997842 H 0.07867133477779 2.37543003877187 0.40525423263047 H -0.64419891613737 4.01255213981484 0.39460421969623 H -0.86325829046916 2.91245092404799 -1.01392900398315 H -4.48998726246165 2.98691991750628 0.48840544517905 H -3.49229506831184 3.26151223530674 -0.96736687424942 H -3.36242163141245 4.37572891756167 0.44113596413710	E = -20628.714270073058 $E_{B97\text{-}D3/def2\text{-}TZVP\ ZORA}$ = -20621.812998021436

Name: $AuBr_4$	**Method:** B97-3c
Optimized geometry (xyz) format	**Energies (Hartree)**
5 Coordinates from ORCA-job orca Au -2.28531972059212 0.72882100660031 0.00000000000000 Br -0.38726999225893 2.33440350361579 0.00000000000000 Br -3.89090639280162 2.62686987498047 0.00000000000000 Br -4.18336553617931 -0.87676125449901 0.00000000000000 Br -0.67973835816803 -1.16922313069757 0.00000000000000	E = -10436.615707302137 $E_{B97\text{-}D3/def2\text{-}TZVP\ ZORA}$ = -30182.324683100625

Name: $AuBr_4$	**Method:** B97-D3/def2-TZVP
Optimized geometry (xyz) format	**Energies (Hartree)**
5 Coordinates from ORCA-job orca Au -2.28532055703638 0.72882290064829 0.00000000000000 Br -0.37728265208346 2.34285703663103 0.00000000000000 Br -3.89935382214637 2.63685709723344 0.00000000000000 Br -4.19336128608535 -0.88520993584195 0.00000000000000 Br -0.67128168264845 -1.17921709867081 0.00000000000000	E = -10438.192855399890 $E_{B97\text{-}D3/def2\text{-}TZVP\ ZORA}$ = -30182.324483323449

Name: $AuBr_4$	**Method:** B97-D3/def2-TZVP ZORA
Optimized geometry (xyz) format	**Energies (Hartree)**
5 Coordinates from ORCA-job orca Au -2.28532038110418 0.72882186035444 0.00000000000000 Br -0.38297218704329 2.33804324433936 0.00000000000000 Br -3.89454097953886 2.63117011903057 0.00000000000000 Br -4.18766874120031 -0.88039936031591 0.00000000000000 Br -0.67609771111336 -1.17352586340848 0.00000000000000	E = -30189.202579219454 $E_{B97\text{-}D3/def2\text{-}TZVP\ ZORA}$ = -30182.324626843085

Name: $AuCl_4$	**Method:** B97-3c
Optimized geometry (xyz) format	**Energies (Hartree)**
5 Coordinates from ORCA-job orca Au -2.28532310072116 0.72882763597323 0.00000000000000 Cl -0.49455886155413 2.24366694432049 0.00000000000000 Cl -3.80014442433885 2.51958257176052 0.00000000000000 Cl -4.07610252791633 -0.78600825294815 0.00000000000000 Cl -0.77047108546953 -1.06195889910610 0.00000000000000	E = -1976.827124067137 $E_{B97\text{-}D3/def2\text{-}TZVP\ ZORA}$ = -21529.618198491662

Name: $AuCl_4$	**Method:** B97-D3/def2-TZVP
Optimized geometry (xyz) format	**Energies (Hartree)**
5 Coordinates from ORCA-job orca Au -2.28531989945178 0.72882130199634 0.00000000000000 Cl -0.49602108427649 2.24241193410656 0.00000000000000 Cl -3.79891180993619 2.51811989375800 0.00000000000000 Cl -4.07461574860053 -0.78476865617253 0.00000000000000 Cl -0.77173145773502 -1.06047447368837 0.00000000000000	E = -1977.226617368620 $E_{B97\text{-}D3/def2\text{-}TZVP\ ZORA}$ = -21529.618248769661

Name: $AuCl_4$	**Method:** B97-D3/def2-TZVP ZORA
Optimized geometry (xyz) format	**Energies (Hartree)**
5 Coordinates from ORCA-job orca	E = -21536.519406448006

Au -2.28532011315608 0.72882152860498 0.00000000000000 Cl -0.50207817636279 2.23728913185210 0.00000000000000 Cl -3.79378785835063 2.51206381429212 0.00000000000000 Cl -4.06856084537248 -0.77964572611415 0.00000000000000 Cl -0.77685300675803 -1.05441874863506 0.00000000000000	$E_{B97\text{-}D3/def2\text{-}TZVP\ ZORA}$ = -21529.618393041063

Name: AuF_4	**Method:** B97-3c
Optimized geometry (xyz) format	**Energies (Hartree)**
5 Coordinates from ORCA-job orca Au -2.28532299207583 0.72882436344964 0.00000000000000 F -0.78490170598572 1.99804233313973 0.00000000000000 F -3.55454716411691 2.22923547569650 0.00000000000000 F -3.78574222760395 -0.54039245681901 0.00000000000000 F -1.01609591021758 -0.77158971546685 0.00000000000000	E = -535.345648200562 $E_{B97\text{-}D3/def2\text{-}TZVP\ ZORA}$ = -20079.431663672392

Name: AuF_4	**Method:** B97-D3/def2-TZVP
Optimized geometry (xyz) format	**Energies (Hartree)**
5 Coordinates from ORCA-job orca Au -2.28531859581418 0.72882247771761 0.00000000000000 F -0.78951943250524 1.99413868019061 0.00000000000000 F -3.55063793026154 2.22462550403418 0.00000000000000 F -3.78112328937814 -0.53649855341125 0.00000000000000 F -1.02000075204089 -0.76697810853115 0.00000000000000	E = -535.484334634162 $E_{B97\text{-}D3/def2\text{-}TZVP\ ZORA}$ = -20079.431870805180

Name: AuF_4	**Method:** B97-D3/def2-TZVP ZORA
Optimized geometry (xyz) format	**Energies (Hartree)**
5 Coordinates from ORCA-job orca Au -2.28532233625775 0.72882395734868 0.00000000000000 F -0.79563761659368 1.98896646105335 0.00000000000000 F -3.54546503317855 2.21850812692754 0.00000000000000 F -3.77500636896599 -0.53131886938029 0.00000000000000 F -1.02517864500402 -0.76085967594928 0.00000000000000	E = -20086.336058291094 $E_{B97\text{-}D3/def2\text{-}TZVP\ ZORA}$ = -20079.431993559454

Name: $AuCl_3$	**Method:** B97-3c
Optimized geometry (xyz) format	**Energies (Hartree)**
4 Coordinates from ORCA-job orca Au -2.78591833476469 0.46802048650111 0.00000000000000 Cl -1.01818104885060 1.89721309241990 0.00000000000000 Cl -4.43766193867869 2.04084470819057 0.00000000000000 Cl -1.59758957770602 -1.47881498711158 0.00000000000000	E = -1516.488046321437 $E_{B97\text{-}D3/def2\text{-}TZVP\ ZORA}$ = -21066.933382478474

Name: $AuCl_3$	**Method:** B97-D3/def2-TZVP
Optimized geometry (xyz) format	**Energies (Hartree)**
4 Coordinates from ORCA-job orca Au -2.78568644296940 0.46813637362996 0.00000000000000 Cl -1.02602775785831 1.89114140699425 0.00000000000000 Cl -4.43193130637790 2.04161472601542 0.00000000000000 Cl -1.59570539279439 -1.47362920663962 0.00000000000000	E = -1516.795883117422 $E_{B97\text{-}D3/def2\text{-}TZVP\ ZORA}$ = -21066.933565103336

Name: $AuCl_3$	**Method:** B97-D3/def2-TZVP ZORA
Optimized geometry (xyz) format	**Energies (Hartree)**
4 Coordinates from ORCA-job orca Au -2.78054172051185 0.46633698404498 0.00000001490014 Cl -1.03891262449699 1.89515484748957 -0.00000000171864 Cl -4.41756958166289 2.03714751480199 -0.00000000657993 Cl -1.60232697332827 -1.47137604633653 -0.00000000660157	E = -21073.835016959914 $E_{B97\text{-}D3/def2\text{-}TZVP\ ZORA}$ = -21066.933742526871